

**ISTANBUL TECHNICAL UNIVERSITY ★ GRADUATE SCHOOL OF  
SCIENCE ENGINEERING AND TECHNOLOGY**

**THE DEVELOPMENT OF HEAT STORING NANOCOMPOSITE  
NANOFIBERS**

**M.Sc. THESIS**

**Ezgi Ceren BOZ NOYAN**

**Department of Textile Engineering**

**Textile Engineering Programme**

**Thesis Advisor: Prof. Dr. Emel ÖNDER KARAOĞLU**

**DECEMBER 2015**



**ISTANBUL TECHNICAL UNIVERSITY ★ GRADUATE SCHOOL OF  
SCIENCE ENGINEERING AND TECHNOLOGY**

**THE DEVELOPMENT OF HEAT STORING NANOCOMPOSITE  
NANOFIBERS**

**M.Sc. THESIS**

**Ezgi Ceren BOZ NOYAN  
503131804**

**Department of Textile Engineering**

**Textile Engineering Programme**

**Thesis Advisor: Prof. Dr. Emel ÖNDER KARAOĞLU**



Ezgi Ceren Boz Noyan, a M.Sc. student of ITU Graduate School of Science Engineering and Technology student ID 503131804, successfully defended the thesis entitled “The Development of Heat Storing Nanocomposite Nanofibers”, which she prepared after fulfilling the requirements specified in the associated legislations, before the jury whose signatures are below.

**Thesis Advisor :**     **Prof. Dr. Emel ÖNDER KARAOĞLU**     .....  
İstanbul Technical University

**Jurry Members :**     **Prof. Dr. Nihal SARIER**     .....  
İstanbul Kültür University

**Prof. Dr. Cevza CANDAN**     .....  
İstanbul Technical University

**Date of Submission :** 27 November 2015

**Date of Defense :** 25 December 2015



*To my family and spouse,*





## **FOREWORD**

I would like to thank, my advisor Dear Prof. Dr. Emel ÖNDER KARAOĞLU for her guidance throughout my thesis with sharing her knowledge and experience during my whole study. Also, I am very thankful to Dear Prof. Dr. Nihal SARIER for her supervision and supports during my thesis. I would like to thank, Refik ARAT for him help and support during laboratory studies at IKU.

I would like to thank, İstanbul Kültür University for their supports about characterizations. I would like to thank, Yıldız Technical University Central Laboratory for SEM analysis and Middle East Technical University Central Laboratory for NMR analysis. I also acknowledge that this thesis has been carried out under The Scientific & Technical Research Council of Turkey (TUBITAK) 213M281 project.

Finally, I would like to thank my friends, my family and my spouse for their precious support throughout my thesis.

December 2015

Ezgi Ceren Boz Noyan  
Textile Engineer



## TABLE OF CONTENTS

	<u>Page</u>
<b>FOREWORD</b> .....	vii
<b>TABLE OF CONTENTS</b> .....	ix
<b>ABBREVIATIONS</b> .....	xi
<b>SYMBOLS</b> .....	xiii
<b>LIST OF TABLES</b> .....	xv
<b>LIST OF FIGURES</b> .....	xvii
<b>SUMMARY</b> .....	xix
<b>ÖZET</b> .....	xxi
<b>1. INTRODUCTION</b> .....	<b>1</b>
1.1 General Information .....	1
1.2 Purpose of Thesis .....	2
<b>2. LITERATURE REVIEW</b> .....	<b>3</b>
2.1 Phase Change Materials for Thermal Energy Management.....	3
2.1.1 Thermal behavior of phase change materials.....	3
2.1.2 Characteristics and classification of PCMs.....	4
2.1.2.1 Inorganic PCMs .....	6
2.1.2.2 Organic PCMs.....	6
Paraffin waxes ( <i>n</i> -alkanes).....	6
Polyethylene glycols (PEGs) .....	7
Polyethylene glycol methyl ethers (PEGMEs) .....	7
Fatty acids and fatty acid derivatives .....	7
Polyalcohols and polyalcohol derivatives.....	8
2.1.3 Storage methods of PCM and their applications.....	8
2.1.3.1 Storage methods.....	8
Microencapsulation of PCMs .....	8
Foam formation.....	9
Shape stabilization .....	9
Electrospinning .....	10
2.1.3.2 Applications .....	10
2.2 Electrospinning .....	11
2.2.1 Method of electrospinning .....	11
2.2.2 The use of PAN in electrospinning .....	14
2.2.2.1 Polyacrylonitrile (PAN) .....	14
2.2.2.2 PAN applications by electrospinning.....	15
2.2.3 PCM applications via electrospinning .....	16
<b>3. MATERIAL AND METHODS</b> .....	<b>17</b>
3.1 Materials.....	17
3.1.1 Core materials .....	17
3.1.1.1 Polyethylene glycols .....	17
3.1.1.2 Polyethylene glycol methyl ethers .....	18
3.1.1.3 Paraffin waxes ( <i>n</i> -alkanes).....	18

3.1.2 Shell materials .....	19
3.1.2.1 Supplied polymers .....	19
3.1.2.2 Synthesized polymers .....	19
3.2 Experimental Study .....	20
3.2.1 Polymer synthesis .....	20
3.2.2 Electrospinning process .....	22
3.3 Characterization .....	26
3.3.1 Structural analysis .....	26
3.3.1.1 Fourier transform infrared spectroscopy (FTIR) .....	26
3.3.1.2 Nuclear magnetic resonance spectrometry (NMR) .....	26
3.3.1.3 Scanning electron microscope (SEM) .....	27
3.3.2 Thermal analysis .....	27
3.3.2.1 Differential scanning calorimetry (DSC) .....	27
3.3.3 Characterization of solutions used in electrospinning .....	29
3.3.3.1 Electrical conductivity analysis .....	29
3.3.3.2 Viscosity analysis .....	29
<b>4. RESULTS .....</b>	<b>31</b>
4.1 Characteristics of Shell and Core Solutions .....	31
4.2 Structural Analysis Results .....	32
4.2.1 Nuclear magnetic resonance spectrometry (NMR) results of synthesized copolymers .....	32
4.2.2 Scanning electron microscope (SEM) results of produced nanowebs .....	33
4.2.2.1 SEM of PAN/PEG nanowebs .....	33
4.2.2.2 SEM of PAN/PEGME nanowebs .....	35
4.2.2.3 SEM of PAN/ <i>n</i> -alkane nanowebs .....	37
4.2.2.4 SEM of nanowebs produced from synthesized copolymers .....	38
4.2.3 Fourier transform infrared spectroscopy (FTIR) results .....	39
4.2.3.1 FTIR of PAN/PEG nanowebs .....	39
4.2.3.2 FTIR of PAN/PEGME anowebs .....	41
4.2.3.3 FTIR of PAN/ <i>n</i> -alkane nanowebs .....	42
4.2.3.4 FTIR of synthesized copolymers and nanowebs produced from them .....	43
4.3 Thermal Characterization Results .....	44
4.3.1 Differential scanning calorimetry (DSC) results of core materials .....	44
4.3.2 Differential scanning calorimetry (DSC) results of nanowebs .....	45
4.3.2.1 DSC of PAN nanowebs .....	45
4.3.2.2 DSC of PAN/PEG nanowebs .....	45
4.3.2.3 DSC of PAN/PEGME nanowebs .....	50
4.3.2.4 DSC of PAN/ <i>n</i> -alkane nanowebs .....	52
4.3.2.5 DSC of nanowebs produced from synthesized grafted copolymers .....	53
<b>5. CONCLUSIONS AND RECOMMENDATIONS .....</b>	<b>53</b>
<b>REFERENCES .....</b>	<b>59</b>
<b>CURRICULUM VITAE .....</b>	<b>63</b>

## **ABBREVIATIONS**

<b>AIBN</b>	: Azobisisobutyronitrile
<b>AN</b>	: Acrylonitrile
<b>DMAc</b>	: Dimethyl acetamide
<b>MAH</b>	: Maleic anyhdride
<b>PAN</b>	: Polyacrylonitrile
<b>PCM</b>	: Phase Change Material
<b>PEG</b>	: Polyethylene glycol
<b>PEGME</b>	: Polyethylene glycol methyl ether
<b>PTSA</b>	: p-Toluenesulfonic acid



## SYMBOLS

$c_{\text{solid}}$ <b>or</b> $c_{\text{liquid}}$	: Specific Heat Capacity
$\Delta H_{\text{fus}}$	: Latent Heat of Fusion
$T_{\text{m}}$ <b>or</b> $T_{\text{g}}$	: Melting Temperature
$M_{\text{w}}$	: Molecular weight
$M_{\text{avg}}$	: Average Molecular Mass
wt%	: Percentage by Weight
$C_{\text{p}}$	: Specific Heat
$Q$	: Heat Added
$m$	: Mass of Material
$\Delta T$	: Change in Temperature
$T_{\text{onset}}$	: Onset Temperature
$T_{\text{peak}}$	: Peak Temperature
$T_{\text{end}}$	: End Temperature





## LIST OF TABLES

	<u>Page</u>
<b>Table 2.1</b> : Important characteristics of PCMs suitable for thermal energy storage. ..	<b>5</b>
<b>Table 2.2</b> : The parameters that effect the electrospinning process. ....	<b>13</b>
<b>Table 3.1</b> : Characteristics of selected PEGs. ....	<b>18</b>
<b>Table 3.2</b> : Characteristics of selected PEGMEs. ....	<b>18</b>
<b>Table 3.3</b> : Characteristics of selected <i>n</i> -alkanes. ....	<b>19</b>
<b>Table 3.4</b> : The materials used in the synthesis and their properties.....	<b>20</b>
<b>Table 3.5</b> : The used parameters in the electrospinning process of shell/core nanowebs. .....	<b>24</b>
<b>Table 3.6</b> : The used parameters in the electrospinning process of hollow nanofibers. .....	<b>26</b>
<b>Table 4.1</b> : Viscosity and conductivity results of shell and core solutions. ....	<b>31</b>
<b>Table 4.2</b> : DSC results of PCMs for 2 <sup>nd</sup> and 10 <sup>th</sup> cycles.....	<b>44</b>
<b>Table 4.3</b> : The DSC results of D1 and D2 nanowebs as 4 <sup>th</sup> cycle. ....	<b>53</b>
<b>Table 5.1</b> : The nanoweb compositions and their corresponding application region. .....	<b>56</b>
<b>Table 5.2</b> : The encapsulation ratio of PCMs for nanoweb having highest enthalpy value among its PAN/PCM composition. ....	<b>56</b>



## LIST OF FIGURES

	<u>Page</u>
<b>Figure 2.1</b> : The sensible and latent heat storage of solid-liquid phase change material. .....	3
<b>Figure 2.2</b> : Classification of heat storage materials. ....	4
<b>Figure 2.3</b> : Classification of microencapsulation techniques. ....	8
<b>Figure 2.4</b> : Schematic diagram of the electrospinning setup. ....	11
<b>Figure 2.5</b> : Schematic diagram of the coaxial electrospinning setup. ....	12
<b>Figure 2.6</b> : Effect of parameters on electrospinning process: (a) Solution parameters. (b) Process parameters.....	13
<b>Figure 3.1</b> : The general chemical formula of PEGs.....	17
<b>Figure 3.2</b> : The general chemical formula of PEGMEs.....	18
<b>Figure 3.3</b> : The general chemical formula of paraffin waxe ( <i>n</i> -alkane). ....	19
<b>Figure 3.4</b> : The chemical formula of PAN. ....	19
<b>Figure 3.5</b> : The chemical formula of a) MAH, b) PEG. ....	20
<b>Figure 3.6</b> : The chemical formula of: (a) AN. (b) Poly(AN).....	21
<b>Figure 3.7</b> : The chemical reaction of PEG-MAH esterification. ....	21
<b>Figure 3.8</b> : The chemical reaction of the graft copolymer PEG-MAH-g-PAN.....	22
<b>Figure 3.9</b> : YFlow® coaxial electrospinning device. ....	22
<b>Figure 3.10</b> : Schematic of simple and double polarized systems. ....	23
<b>Figure 3.11</b> : The Taylor cone visualization system. ....	23
<b>Figure 3.12</b> : Schematic of coaxial design. ....	24
<b>Figure 3.13</b> : PerkinElmer DSC4000 machine.....	28
<b>Figure 4.1</b> : <sup>1</sup> HNMR graphs of synthesized PEG1000-MAH-g-PAN and PEG1500- MAH-g-PAN copolymers. ....	32
<b>Figure 4.2</b> : <sup>13</sup> CNMR graphs of synthesized PEG1000-MAH-g-PAN and PEG1500- MAH-g-PAN copolymers. ....	33
<b>Figure 4.3</b> : (a) SEM image of 6S40CPEG13 nanoweb. (b) Diameter distribution histogram of 6S40CPEG13 nanoweb. ....	34
<b>Figure 4.4</b> : (a) SEM image of 4S30CPEG9 nanoweb. (b) Diameter distribution histogram of 4S30CPEG9 nanoweb. ....	34
<b>Figure 4.5</b> : (a) SEM image of 6S30CPEG23 nanoweb. (b) Diameter distribution histogram of 6S30CPEG23 nanoweb. ....	34
<b>Figure 4.6</b> : (a) SEM image of 4S40CPEG6 nanoweb. (b) Diameter distribution histogram of 4S40CPEG6 nanoweb. ....	35
<b>Figure 4.7</b> : (a) SEM image of 6S20CPEGME7 nanoweb. (b) Diameter distribution histogram of 6S20CPEGME7nanoweb. ....	36
<b>Figure 4.8</b> : (a) SEM image of 4S30CPEGME2 nanoweb. (b) Diameter distribution histogram of 4S30CPEGME2 nanoweb. ....	36
<b>Figure 4.9</b> : (a) SEM image of 6S100CPW2 nanoweb. (b) Diameter distribution histogram of 6S100CPW2 nanoweb. ....	37
<b>Figure 4.10</b> : (a) SEM image of 6S100CPW3 nanoweb. (b) Diameter distribution histogram of 6S100CPW3 nanoweb. ....	37

<b>Figure 4.11</b> :	(a) SEM image of D1 nanoweb. (b) Diameter distribution histogram of D1 nanoweb. ....	<b>38</b>
<b>Figure 4.12</b> :	(a) SEM image of D2 nanoweb. (b) Diameter distribution histogram of D2 nanoweb. ....	<b>38</b>
<b>Figure 4.13</b> :	The comparative FTIR spectra of: (a) 4S, PEG400 and 4S/PEG400 nanoweb. (b) 6S, PEG400 and 6S/PEG400 nanoweb. ....	<b>39</b>
<b>Figure 4.14</b> :	The comparative FTIR spectra of: (a) 4S, PEG1500 and 4S/PEG1500 nanoweb. (b) 6S, PEG1500 and 6S/PEG1500 nanoweb. ....	<b>40</b>
<b>Figure 4.15</b> :	The comparative FTIR spectra of: (a) 4S, PEGME550 and 4S/PEGME550 nanoweb. (b) 4S, PEGME750 and 4S/PEGME750 nanoweb. ....	<b>41</b>
<b>Figure 4.16</b> :	The comparative FTIR spectra of: (a) 6S, <i>n</i> -pentadecane and 6S100CPW2 nanoweb. (b) 6S, <i>n</i> -hexadecane and 6S100CPW3 nanoweb. ....	<b>42</b>
<b>Figure 4.17</b> :	FTIR spectra of (a) D1 nanoweb in comparison with PEG1000-MAH-g-PAN ,pure PAN and PEG1000. (b) D2 nanoweb in comparison with PEG1500-MAH-g-PAN pure PAN and PEG1500. ....	<b>43</b>
<b>Figure 4.18</b> :	The comparative DSC graphs of PAN, 4S and 6S for 2 <sup>nd</sup> cycle; at the rate of 10°C.min <sup>-1</sup> . ....	<b>45</b>
<b>Figure 4.19</b> :	The DSC graphs of PAN/PEG400 nanoweb in comparison with pure PEG400: (a) 4PAN/PEG400 nanoweb. (b) 6PAN/PEG400 nanoweb. ....	<b>46</b>
<b>Figure 4.20</b> :	The DSC graphs of PAN/PEG600 nanoweb in comparison with pure PEG600: (a) 4PAN/PEG600 nanoweb. (b) 6PAN/PEG600 nanoweb. ....	<b>47</b>
<b>Figure 4.21</b> :	The DSC graphs of PAN/PEG1000 nanoweb in comparison with pure PEG1000: (a) 4PAN/PEG1000 nanoweb. (b) 6PAN/PEG1000 nanoweb. ....	<b>48</b>
<b>Figure 4.22</b> :	The DSC graphs of PAN/PEG1500 nanoweb in comparison with pure PEG1500: (a) 4PAN/PEG1500 nanoweb. (b) 6PAN/PEG1500 nanoweb. ....	<b>49</b>
<b>Figure 4.23</b> :	The DSC graphs of PAN/PEGME550 nanoweb in comparison with pure PEGME550: (a) 4PAN/PEGME550 nanoweb. (b) 6PAN/PEGME550 nanoweb. ....	<b>50</b>
<b>Figure 4.24</b> :	The DSC graphs of PAN/PEGME750 nanoweb in comparison with pure PEGME750: (a) 4PAN/PEGME750 nanoweb. (b) 6PAN/PEGME750 nanoweb. ....	<b>51</b>
<b>Figure 4.25</b> :	The DSC graphs of PAN/ <i>n</i> -alkane nanoweb in comparison with corresponding pure <i>n</i> -alkane. ....	<b>52</b>

## **THE DEVELOPMENT OF HEAT STORING NANOCOMPOSITE NANOFIBERS**

### **SUMMARY**

Thermal management applications are gained importance increasingly in the last decade due to the changings in climates, demand for developed energy conservation as well as improved thermal comfort. Thus, investigation and improvement cost effective, ecologically friendly and simple methods have been the focus of attention by researchers. Organic phase change materials (PCMs), which have the ability to absorb and release large quantities of latent heat during a phase change process, offer remarkable potential to fulfill the growing energy requirements for cooling and heating applications across various industries, including construction, refrigeration, textiles, packaging, solar energy systems, electronics and biomedical materials.

A variety of encapsulating and storage processes have been applied to PCMs before integrating them into different composites to prevent their interaction with the surrounding medium, to increase their mechanical and thermal stabilities and to enhance their ease of handling. Recently, the electrospinning technique has been employed as a simple, convenient, and versatile technique for generating form-stable PCMs.

In this study, production of bicomponent nanowebs, composed of polyacrylonitrile (PAN) shells and PCM cores were performed via coaxial electrospinning method. Moreover, PCM grafted PAN copolymers were synthesized with developing unique recipe than used as a shell material to produce composite hollow nanofibers.

Polyacrylonitrile (PAN) was preferred for its very good thermal stability, high tensile strength and elastic modulus, low density, high moisture management and excellent thermal insulation properties. Polyethylene glycols (PEG), polyethylene glycol methyl ethers (PEGME) and paraffin waxes (*n*-alkane) were preferred as a PCM to use in the core because of their high latent heat capacities, chemical and thermal stability and ecological friendly properties.

The experimental part of the study consist of; determining the appropriate solvents and concentrations of shell and core solutions for electrospinning experiment, synthesis of PCM grafted PAN copolymer and characterizations of them, producing bicomponent nanowebs composed of PAN/PCM as a shell/core with using different concentrations of shell and core solutions, lastly characterizations of produced nanowebs.

4wt% PAN and 6wt% PAN solutions were chosen as a shell material due to better processibility and different concentrations of core materials were used related with their own properties. Synthesized grafted copolymer used in a mixture of shell solution to produce hollow nanofibers. After several trials and fine tuning electrospinning parameters were modified for each pair of shell/core combination.

Structural and thermal characterizations of each core and shell material as well as produced nanowires were performed. Structural properties were determined with fourier transform infrared spectroscopy (FTIR) and thermal behavior were carried out with differential scanning calorimetry (DSC). In addition, nuclear magnetic resonance (NMR) analysis were conducted for synthesized grafted copolymers. Surface images of produced nanowires were characterized with scanning electron microscopy (SEM) and diameter distribution analysis also performed by ImageJ-DiameterJ program. Also conductivity and viscosity analysis were performed for core and shell solutions.

The obtained structural and thermal characterization results showed that desired nanowires having thermal management feature were achieved for all produced nanowire composition.

## ISI DEPOLAYABİLEN NANOKOMPOZİT NANOLİFLERİN GELİŞTİRİLMESİ

### ÖZET

Son yıllarda giderek değişen iklim koşulları ve buna bağlı olarak değişen çevre şartları nasıl binalarda, güneş enerji sistemlerinde ısı yönetimi yapabilmenin önemini arttırdı ise tekstil endüstrisinde de gerek teknik ve akıllı tekstil uygulamalarında gerekse günlük giysi olarak tekstil kullanımında ısı yönetiminin önemini, gereksinimini arttırmıştır. Isı yönetimi yapabilme amacı ile otomatik olarak çevreye uyum sağlama yeteneğine sahip olan lif ve diğer tekstil ürünleri giderek dikkat çekmektedir ve bu konuya olan ilgi giderek artmaktadır. Bununla beraber enerji depolama kapasitesi ve ısıl kararlılığı yüksek, çok ince ve esnek malzemelerin üretilebilmesine yönelik bilimsel ve endüstriyel ilgi giderek önem kazanmaktadır ve elektroğirme yöntemi sahip olduğu üstün özellikleri ile bu kapsamda son yıllarda öne çıkmaktadır.

Faz değiştiren malzeme (FDM) kullanımı ile tekstil ürünün ısı yönetimi yapabilme kabiliyetini geliştirmek mümkün olabilmektedir ve bu kapsamda yapılan çalışmalar giderek artan ilgi ve önemle devam etmektedir. FDM'ler belli sıcaklık aralıklarında katı-katı veya katı-sıvı faz geçişi sırasında ortamdan ciddi bir oranda enerji absorplayıp, depolayabilen ve depoladığı bu enerjiyi geri salabilen özelliğe sahip malzemelerdir. Bu nedenle güneş enerji sistemlerinde, binalarda, termoregülasyon tesislerinde, gıda ve kan taşımada, sıcak-soğuk terapilerinde çok geniş kullanım alanı bulan faz değiştiren malzemeler (FDM) tekstilde de spor giysisi, koruyucu giysi, ayakkabılarda termo regülasyon amaçlı kullanım alanına sahiptir. Isı yönetiminde FDM kullanımı hala güncel bir konudur ve bu kapsamda yapılan çalışmalar devam etmektedir.

Bu çalışma, kullanım alanı giderek yaygınlaşan ve çalışmalarına halen devam edilmekte olan elektroğirme yöntemi ile ısı depolayabilen nanolif ağların üretilebilme olanaklarını araştırması bakımından farklılık göstermektedir. Çalışmada, tekstil lifi olarak çok yaygın kullanım alanı bulunan akrilik liflerin hammaddesi olan PAN kopolimeri ile biyoesaslı ve yenilenebilir kaynaklardan üretilebilen organik FDM'ler kullanılarak eşeksenli çift düze sistemiyle donatılmış elektroğirme tekniği ile kabuk/öz kompozit nanoliflerden oluşan nanoağlar üretilmiştir. Ek olarak FDM aşılınmış PAN kompozit yapılı nanoliflerden oluşan nanoağ üretimi de gerçekleştirilmiştir.

PAN lifleri sahip oldukları iyi mekanik özellikleri, kimyasal kararlılığı, yüksek nem yönetim kabiliyeti sayesinde kabuk malzemesi olarak tercih edilmiştir. Öz malzeme olarak kullanılmak üzere FDM'lerden polietilen glikoller (PEG), polietilen glikol metil eterler (PEGME) ve parafin vaksları (*n*-alkan) sahip oldukları yüksek ısı kapasiteleri, kimyasal ve termal kararlılıkları, ekolojik olarak zararsız olma özellikleri bakımından tercih edilmişlerdir.

Deneyisel çalışma; elektroğirmeye kullanılacak kabuk ve öz malzemeler için laboratuvar ortamında uygun çözücü ve derişimlerinin belirlenmesi, hazır alınan PAN kopolimerinin yanısıra kabuk malzemesi olarak kullanılması tasarlanan FDM aşılınmış PAN polimerinin özgün reçete oluşturularak sentezlenmesi ve üretilen malzemenin karakterizasyonun yapılması, kullanılacak kabuk/öz varyasyonlarının belirlenerek PAN/FDM bikomponent nanoliflerin eş eksenli çift düze sistemiyle kontrollü şartlar altında elektroğirmeleri ve üretilen nanoağların karakterizasyonları kısımlarını içermektedir.

Elektroğirme parametreleri yapılan ön denemeler ve ince ayarlar sonucu her bir kabuk/öz için modifiye edilmiş ve Taylor konisi elde edilen aralıklar dikkate alınarak nanoağlar üretilmiştir. Yapılan denemeler sonucu kabuk malzemesi olarak diğerlerine nazaran daha iyi sonuç elde edilen %4 ve %6'lık PAN konsantrasyonları kullanılmıştır. Öz malzemeler için herbirinin kendi yapısı ve elektroğirme uygulamasındaki kolaylık göz önüne alınarak iki farklı konsantrasyon kullanılmıştır. Isı depolayabilme özelliğine sahip içi boş nanaliflerden oluşan nanoağ yapılar elde etmek amacı ile sentezlenen FDM aşılınmış PAN kopolimerin çözeltisi, PAN kopolimer çözeltisi ile karıştırılarak kabuk malzemesi olarak kullanılmıştır.

Çalışmada kullanılan tüm kabuk ve öz malzemeler ile üretilen nanoağların yapısal ve termal karakterizasyonları gerçekleştirilmiştir. Yapısal özellikler Fourier transform infrared spektrofotometre (FTIR), ısıl özellikleri diferansiyel taramalı kalorimetre (DSC) ile karakterize edilmiştir. Bunun yanı sıra sentezlenen polimerlerin nükleer manyetik rezonans (NMR) karakterizasyonları da gerçekleştirilmiştir. Üretilen nanoağların yüzey görüntüleri taramalı elektron mikroskop (SEM) analizi ile elde edilmiş ve bu görüntüler üzerinden ImageJ-DimaeterJ programları kullanılarak çap dağılım grafikleri oluşturulmuştur. Elektroğirmeye kullanılan kabuk ve öz malzemelerin viskozite ve iletkenlik ölçümleri de gerçekleştirilmiştir.

Sentezlenen FDM aşılınmış PAN kopolimerinin, kullanılan FDM ve PAN ile karşılaştırmalı FTIR grafiği sonucunda göstermiş olduğu pikler sentezin başarılı bir şekilde gerçekleştirildiğini ortaya koymaktadır. NMR grafikleri de FTIR sonucunu destekler niteliktedir. Üretilen nanoağlar için de FTIR analizleri üretimde kullanılan ilgili kabuk ve öz malzeme dikkate alınarak karşılaştırmalı olarak değerlendirilmiştir. Analiz sonucunda tüm nanoağların üretildiği PAN ve FDM malzemesinin tipik dalga boylarına sahip olduğu ve hiçbir yeni pikin türemediği görülmüştür. Bu da kabuk ve öz malzemenin elektroğirme sırasında birbirleri ile karışmadığını göstermektedir.

SEM görüntüleri tüm nanoağların çoğunlukla boncuksuz, pürüzsüz ve silindirik nanlif yapılarına sahip olduklarını göstermiştir. Yapılan çap dağılım analizi de maksimum 900 nm'lere ulaşan ortalama çap değerleri ile malzemelerin nano boyutta üretilebildiğini destekler niteliktedir.

Öz malzemelerin ısıl özelliklerini karakterize etmek için DSC cihazı ile gerçekleştirilen on ardışık ısıtma ve soğutma termal çevrim analizi sonucunda herbir FDM'nin kendi on termal çevrimi süresince hem ısıtma hem soğutma proseslerinde faz değişim aralıklarını ve entalpi değerlerini koruduklarını göstermiştir. Elde edilen sonuçlar kullanılan FDM'lerin termal kararlılığa sahip olduğunu ve elektroğirme uygulamasına uygun olduklarını desteklemiştir. Üretilen nanoağların ısıl özellikleri dört ardışık ısıtma ve soğutma termal çevrimi ile karakterize edilmiştir. DSC grafikleri FTIR analizine benzer şekilde üretilen nanoağlar ile ilgili FDM baz alınarak karşılaştırmalı olarak değerlendirilmiştir. DSC analiz sonuçlarına göre, kontrol grubu olarak kullanılmaları amacı ile sadece PAN kabuk malzemesi kullanılarak üretilen



nanoğlar hiçbir faz deęişim ve entalpi deęeri sergilemezken üretilen nanoğların ilgili FDM ile benzer faz deęişim sıcaklık aralıklarında belirli entalpi deęerine sahip oldukları görölmektedir. Bu sonuç ısı depolayabilme kabiliyetine sahip nanoağların üretildiğini destekler niteliktedir.

Bu çalışma, literatürde de henüz çok yeni çalışma alanı olan PAN/FDM kombinasyonlarının elektroęirme yöntemi ile nanolif üretiminde kullanımına farklı bir bakış açısı kazandırma adına özgün bir girişimi içermekte ve yeni çalışmalar açısından potansiyel arz etmektedir.



## **1. INTRODUCTION**

### **1.1 General Information**

In recent years, with gradually changing climates and environmental aspects there is increased attention for effective thermal management in buildings, solar energy systems as well as textile industry. Thus, develop of cost effective, ecologically friendly and simple solutions and methods have been the focus of attention by researchers. Textile fibers and products, with the ability to automatically adapt to the environment in order to provide thermal management, have been increasingly draw attention and such products have been came into prominence.

A phase change material (PCM) is an inorganic or organic compound which is capable of absorbing or releasing great amount of energy in a form of latent heat during phase transitions. Usage of PCMs in thermal management applications have been very widely studied over the years [1]. In the early 1980s, the technology is developed under NASA research program, for integrating PCM microcapsules into textile structure with the aim of improve their thermal performance [2]. The use of PCM for heat storage and thermal management is still a current issue and studies in this respect continues.

Nowadays, there is also attention for producing very thin, flexible materials or products with high energy storage capacity and good thermal stability. The electrospinning method, which is based on converting of viscoelastic fluids into sub-micron or nanometer sized fibers, stands out for the development and production of such material. Electrospinning is a quite simple, practical and flexible method with the advantage of capability of using very wide range of polymers, polymer blends or nanoparticle doped polymer mixtures, to produce nanofibers or nanocomposite nanowebs. The produced nanofibers possesses unique and excellent properties (optically, chemically, mechanically, etc.) and thanks to their high surface area over volume ratio it seems they will have a great importance in industrial application areas such as, filtration, high performance sensor applications, drug delivery, artificial blood

vessels and organs applications, micro/nano devices, thermal insulation applications, solar energy applications, energy storage systems, in the future [3, 4].

## **1.2 Purpose of Thesis**

The aim of the thesis is to design and develop bicomponent shell/core structured nanofiber webs, with high area over volume ratio, which provide some important features as follows;

- High area of heat transfer
- Capability of storing and releasing high amount of heat
- Capability of performing heat store and release action repeatedly
- Ability for transferring this stored heat
- Ability for ensuring the continuity of the microclimate of the environment despite changes in outside temperatures.

In this study, homopolymers and/or copolymers of polyacrylonitrile (PAN), which is widely used as the raw material in the manufacture of acrylic fibers in textile, will be incorporated with the bio-based and renewable phase change materials (PCMs) in order to produce various nanofiber based new composites using an electrospinning system provided with both single and coaxial nozzles of different characteristics. This point of view, will improve and diverse the usage of PAN and PCMs in thermal management applications, thanks to the advantages of electrospinning.

With this purpose, the production of nanowebs with bicomponent shell/core nanofibers using PAN/PCM and with hollow nanofibers using PCM-grafted-PAN composite structures will be performed. The structural, surface and thermal characteristics of produced nanowebs will be tested with appropriate methods. This study includes a unique attempt, on behalf gain a different perspective for usage of PAN-PCM combinations in nanofiber production with electrospinning method which is still very new field of research in the literatures.

## 2. LITERATURE REVIEW

### 2.1 Phase Change Materials for Thermal Energy Management

#### 2.1.1 Thermal behavior of phase change materials

The thermal behavior of materials can be signified in terms of heat capacity and thermal conductivity. Heat capacity is a property that is determinative of a material's ability to absorb heat from the external surroundings. When a solid material heated, experiences an increase in temperature indicating that some energy has been absorbed. The heat absorbed by one gram of a solid material to produce a unit temperature rise is defined as its specific heat capacity ( $c_{\text{solid}}$ ). In thermal storage studies, the specific heat capacity of a substance is commonly named as sensible heat.

During melting, the heat absorbed by a solid is consumed to break up the physical bonds within its crystal structure. Therefore, solid and liquid phases exist together during melting and the temperature of the system remains constant until all of the solid particles became liquid. The heat capacity of melting is named as the latent heat of fusion ( $\Delta H_{\text{fus}}$ ) or latent heat of phase transition. As heating continues, the temperature of the liquid rises and the corresponding heat absorbed by one gram of liquid to rise a unit temperature is called its specific heat capacity ( $c_{\text{liquid}}$ ) [5]. Figure 2.1 shows both sensible and latent heat storages plotted against the temperature during solid-liquid phase change of a material.

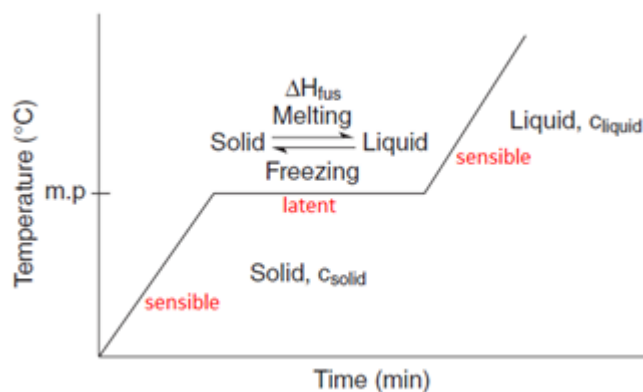


**Figure 2.1 :** The sensible and latent heat storage of solid-liquid phase change material [5].

Latent heat storage is the most efficient and more attractive method for storing thermal energy as it has the ability to provide a high storage density at nearly isothermal conditions or a small temperature difference between storage and retrieval cycles [2, 6, 7, 8]. However, during cooling process from liquid to solid, there is commonly encountered effect called supercooling. Supercooling, also named as subcooling, is the process of lowering the temperature of a liquid below its freezing point without it becoming a solid. A liquid at its standard freezing point will crystallize around a nucleus of a critical size ( $r_{crit}$ ) which only beyond this value there is possibility for free growth of the new solid phase. Many PCMs have tendency to supercool in microscopic geometries [5].

Besides sensible and latent heat storage there is also thermochemical energy storage, there should be a chemical reaction with high energy contained in the reaction and thus is used to store energy. When a chemical reaction takes place, substances at the start and substances at the end of the reaction have different enthalpies that the difference between enthalpies is known as heat of reaction.

**2.1.2 Characteristics and classification of PCMs**

The use of materials which have high specific heat capacities, high latent heats of phase transition or a combination of both has been rapidly increasing in thermal energy storage applications. Latent heat storage materials, usually known as phase change materials (PCMs), have been receiving great attention during the last 50 years. The use of PCMs is chiefly attractive due to their capability of providing high energy storage density, allowing a compact energy storage system, and having a high heat of phase transition at nearly isothermal conditions [5]. Figure 2.2 indicates general classification of heat storage materials.

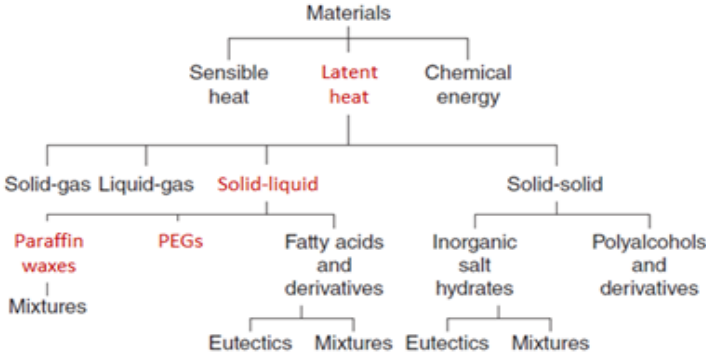


**Figure 2.2** : Classification of heat storage materials [5].

The applications of PCMs with phase transitions of solid-gas or liquid-gas are limited due to their large volume changes associated with the transition which is undesired situation in thermal energy storage applications. Solid-solid or solid-liquid PCMs have significantly smaller volume changes in phase transition that makes them economically and practically more attractive as heat storage materials. In solid-solid phase change there is a phase transition one to another crystalline form and can be considered as an alternative to solid-liquid PCMs however heat of phase transition for solid-solid PCMs is lower than solid-liquid PCMs [7].

PCM should fulfill some requirements for most but not all applications in order to use in thermal energy storage effectively. These requirements are listed below in Table 2.1 under thermal, physical, chemical and economic aspects. These characteristics are important to choose and use most suitable PCM according to where it would be use.

**Table 2.1 :** Important characteristics of PCMs suitable for thermal energy storage [5].

<b>Property</b>	<b>Requirements</b>
<b>Thermal</b>	<ol style="list-style-type: none"> <li>1. Suitable phase change temperature interval for the practical range of application</li> <li>2. High enthalpy of phase change</li> <li>3. High specific heat capacity to provide additional heat storage</li> <li>4. Reproducible phase change</li> <li>5. Thermal cycling stability</li> <li>6. High thermal conductivity of both solid and liquid phases</li> </ol>
<b>Physical</b>	<ol style="list-style-type: none"> <li>1. High density</li> <li>2. High rate of nucleation or crystallization to avoid supercooling</li> <li>3. Low volume change</li> <li>4. Low vapor pressure</li> <li>5. No segregation during phase changing</li> </ol>
<b>Chemical</b>	<ol style="list-style-type: none"> <li>1. Chemical stability</li> <li>2. Non-toxic</li> <li>3. Non-flammable</li> <li>4. Non-explosive</li> <li>5. Non-corrosive</li> <li>6. Compatible with hpst material</li> <li>7. Environmental friendly based on life cycle assessment</li> </ol>
<b>Economic</b>	<ol style="list-style-type: none"> <li>1. Abundant</li> <li>2. Available in the markets</li> <li>3. Cost effective</li> <li>4. Appropriate for recycling</li> </ol>

As a latent heat storage material general classification of PCMs can be seen from Figure 2.2, the red ones which are paraffin waxes and poly(ethylene glycol)s and derivatives are our preferred PCMs in this study. The characteristic information about various PCMs are given below, under classification of inorganic and organic PCMs.

### 2.1.2.1 Inorganic PCMs

An inorganic salt hydrates is a crystal lattice which consists of ions and a number of water molecules attracted by these ions and represented by general formula of  $M_xN_y.nH_2O$ . They demonstrate solid-solid phase transition and the principle of phase change is, during heating a certain amount of energy absorbed by hydrated salt as it loses its water of crystallization, while cooling these energy released with capture of water molecules from the surroundings by salt crystals. Hydrated salts have some advantages such as, high latent heat of phase change per unit volume, relatively high thermal conductivity (almost double that of paraffin waxes), small volume change on dehydration and hydration, compatibility with many thermoplastics, and non-toxicity. However, they have notable disadvantage of phase separation that limit their application in thermal storage as they show problems with cycling stability [5].

### 2.1.2.2 Organic PCMs

The well-known and widely studied organic PCMs, which undergo solid–liquid phase transition during heating and subsequent cooling, are paraffin waxes, poly(ethylene glycol)s, fatty acids and their derivatives. Moreover, a group of organic PCMs, such as polyalcohols and derivatives, which submit to solid–solid phase transition at a constant temperature by absorbing and releasing a large amount of latent heat, have attracted attention as promising organic PCMs [5].

#### Paraffin waxes (*n*-alkanes)

The paraffin waxes are one of the most important groups of organic PCMs represented by the generalized formula  $C_nH_{2n+2}$ , where  $n$  varies between 12 and 28 over the temperature range from  $-10^\circ\text{C}$  to  $61^\circ\text{C}$  that makes them suitable for many heat storage applications. Paraffin waxes absorb, store and release a great amount of heat repeatedly during phase changes between solid-liquid phases, they have considerably high latent heat storage capacities  $\Delta H_{\text{fus}}$ , between  $140 \text{ kJ.kg}^{-1}$  and  $260 \text{ kJ.kg}^{-1}$ , with a wide range of melting temperatures and a thermal stability up to  $250^\circ\text{C}$ . The melting temperature ( $T_m$ ) of a paraffin wax increases with an increasing chain length, for instance the melting point of *n*-dodecane (12C atoms) is  $-10^\circ\text{C}$ , while *n*-nonadecane (19C atoms) is  $32^\circ\text{C}$ . Supercooling, which means that the crystallization temperature of a material is slightly lower than its melting temperature and low thermal conductivity ( $k$ ) are disadvantages of paraffin waxes. However, they display no phase segregation during



repetitive phase transitions. They are chemically inert, non-corrosive, odorless, long lasting, inexpensive, easily available, ecologically harmless and non-toxic. [1].

### **Polyethylene glycols (PEGs)**

PEGs are composed of linear dimethyl ether chains with hydroxyl ending groups,  $\text{HO}-\text{CH}_2-(\text{CH}_2-\text{O}-\text{CH}_2)_n-\text{CH}_2-\text{OH}$ , and accordingly possess dual feature of water solubility and organic solubility. The molecular weight ( $M_w$ ) of PEG varies with  $n$ , thus there are various PEG in different average molar mass ( $M_{\text{avg}}$ ). The melting temperatures and the values of latent heat of fusion of PEGs increase gradually with increase of the  $M_{\text{avg}}$  of the PEG chains. PEG compounds and their mixtures have attracted attention for diverse thermal storage applications, which range from building envelopes to fabrics, foams and fibers, because of their desirable characteristics, such as high heat of fusion, low and moderate melting temperature intervals, low vapor pressure when melted, and because they are chemically and thermally stable, biodegradable, non-toxic, non-corrosive and inexpensive. Though, they commonly demonstrate a considerable supercooling effect due to the difficulty of crystallization of long PEG chains during cooling. [1].

### **Polyethylene glycol methyl ethers (PEGMEs)**

PEGME can be expressed as a derivative of PEG and they are addition polymers of ethylene oxide and methanol. Its general formula is  $\text{CH}_3\text{O}-(\text{CH}_2-\text{CH}_2-\text{O})_n-\text{H}$ , with a little difference from PEG that there is  $\text{CH}_3$  group in one end rather than H. PEGMEs also have a good thermal and chemical stability likewise PEGs with again high heat of fusion as well as they are non-toxic, non-corrosive, biodegradable, soluble in water, easy to handle and store [9, 10].

### **Fatty acids and fatty acid derivatives**

Fatty acids are represented by the formula  $\text{CH}_3(\text{CH}_2)_{2n}\text{COOH}$ , there is  $-\text{COOH}$  in one end of the molecule instead of a  $-\text{CH}_3$  group in contrast to a paraffin waxes. Fatty acids and their derivatives have superior properties such as melting congruency, good chemical and thermal stability, non-toxicity, biodegradability and a suitable melting temperature range for several heat storage applications. However, they show bad odor, corrosiveness, and especially high sublimation rate as undesired properties [5].

## Polyalcohols and polyalcohol derivatives

Polyalcohols consists of alcohol and derivatives of 2,2-dimethylpropane (Neopentane, NP) include pentaerythritol (PE), pentaglycerine (PG) and neopentylglycol (NPG). They show solid-solid phase transition and can absorb and release a large amount of heat during the phase transition, reversibly and they also do not show segregation, no leakage, have long lifespan, small volumetric change, and small erosion to the device [5, 8].

### 2.1.3 Storage methods of PCM and their applications

#### 2.1.3.1 Storage methods

There are many studies about to improve usage of PCM effectively by trying to reduce their reactivity with the ambient, decrease their diffusion and evaporation rates and so as to promote ease of handling [1]. There are some developed methods which are microencapsulation, foam formation and shape stabilization. Recently, electrospinning method has been introduced.

#### Microencapsulation of PCMs

A microcapsule consists of core material which can be solid particles, liquid droplets or gas bubbles and shell material which can be polymer or co-polymer that encapsulates this core material. The microcapsules are generally particles that their diameters vary from  $1\mu\text{m}$  to  $1000\mu\text{m}$  [5]. Microencapsulation can be performed via different techniques that are shown in Figure 2.3.

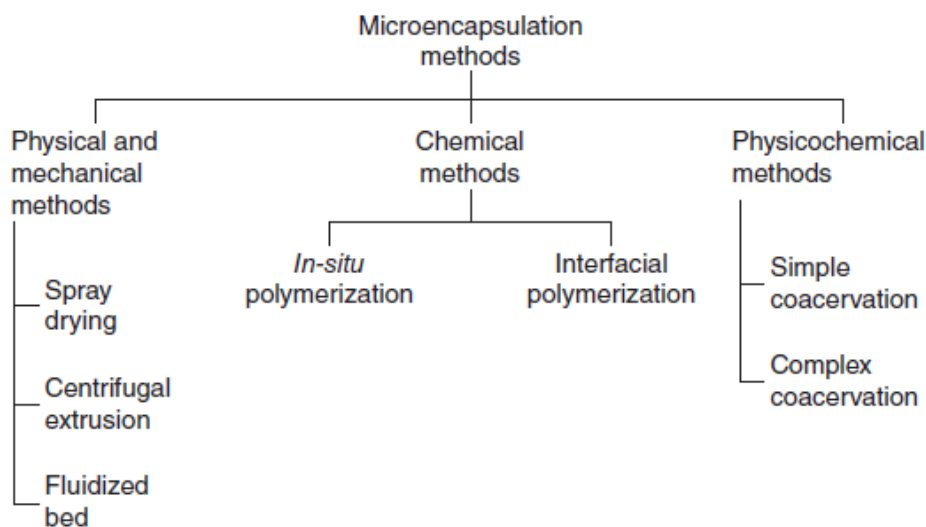


**Figure 2.3** : Classification of microencapsulation techniques [5].

Protection of unstable, sensitive materials from their environments prior to use, better processing by improving solubility and dispersibility of core and shell materials, employment of a variety of core materials, production with a high concentration and high yield, shelf-life enhancement by preventing degradative reactions and evaporation, safe and convenient handling of core materials, masking of odor or taste are the main advantages of microencapsulated PCMs. However, their cost is limited the potential use of such PCMs in thermal control applications. Also they should meet some criteria such as; suitable particle size and thickness of wall, mechanical strength, durability to temperature, humidity and various solvents, functionality over phase transition cycles [1, 5].

### **Foam formation**

This method based on capturing PCM into rigid foam. Polyurethane (PU) foam have been widely used for their great insulation properties which important in thermal energy applications. There are three methods for incorporation of PCM into foam as follows; (i) direct injection and dispersion of PCM, (ii) entrapment of PCMs in composite structure, (iii) chemical grafting or blocking co-polymerization. Incorporation of PCMs into foam has some advantages like, the lowest thermal conductivity, high mechanical and chemical stability at both high and low temperatures and the ability to form sandwich structures with various facer materials [1, 5].

### **Shape stabilization**

These method developed to provide a solution for some disadvantages of microencapsulation process like their cost and leakage problem. New type encased shape stabilized PCMs are tried to achieve with three different technique as follows; (i) by preparing a liquid mixture of PCM and supporting material then cooling below the glass transition temperature of the supporting material, until the mixture becomes solid, (ii) by encapsulating PCMs with inorganic shells, and (iii) by incorporating liquid PCM into the solid matrix. According to some researches there are found advantages about shape stabilized PCM applications, such as large heat capacities for the phase-transition temperature region, suitable thermal conductivity, keeping shape and preventing leakage throughout the phase change process, and no need for containers [1, 5].

## **Electrospinning**

Merely a few types of fibers, which have the feature of thermal management, can be produced by conventional spinning methods due to inadequate processibility for many polymers and PCMs. Recently, electrospinning which is a remarkably simple, convenient and versatile technique, has been introduced to generate ultrafine nano- and micro- scale fibers in large quantities from a wide variety of polymers, polymer blends and nanoparticle impregnated polymers. Electrospun fibers can be functional and usable in numerous areas such as healthcare, biotechnology, environmental engineering and energy storage due to their ultrafine size and huge surface to volume ratio [5]. The review of electrospinning techniques and the important process parameters are given in detail in Section 2.2.

### **2.1.3.2 Applications**

PCMs are capable of using in all areas related with thermal energy. Building industry, automotive sector, solar energy based systems, transportation packaging for temperature-sensitive products, food industry, space applications and textile industry are general usage area of PCMs, in recent years potential using of PCMs in electronics and biomedical applications has emerged also. PCM applications can be used as a smart textile in clothing like firefighter suits, chemical, biological, radiological and nuclear (CBRN) protective clothing, cold-weather protective clothing, sportswear, medical clothing, space suits, bedding and accessories and shoes and there are many studies about usage of PCM in textiles [2, 7, 8, 11].

The phase change material market is expected to grow from \$460 million in 2013 to \$1150 million by 2018, at an estimated compound annual growth rate (CAGR) of 20.1% during the same period. Over the last 20 years, high quality and thermally efficient PCM products have been launched to the market by several companies. Outlast®, PureTemp®, Schoeller®, Microtek Laboratories Inc. are companies that have their own PCM incorporated products commercially. BASF (Germany), Climator AB (Sweden), Cristopia Energy Systems (France), Environmental Process Systems Ltd (UK), Mitsubishi Chemical (Japan), Phase Change Products Pty Ltd (Australia), Rubitherm GmbH (Germany), Teappcm (India) companies which have their commercial PCMs [2, 5, 8, 12].

## 2.2 Electrospinning

### 2.2.1 Method of electrospinning

Electrospinning is a technology which utilizes electrical forces to produce polymer fibers with diameters down to a few nanometers. The basic electrospinning system consists of three major components that are; a spinneret, a grounded collector and a high voltage supplier connected between the spinneret and the collector [13]. The schematic diagram of the electrospinning setup can be seen in Figure 2.4.

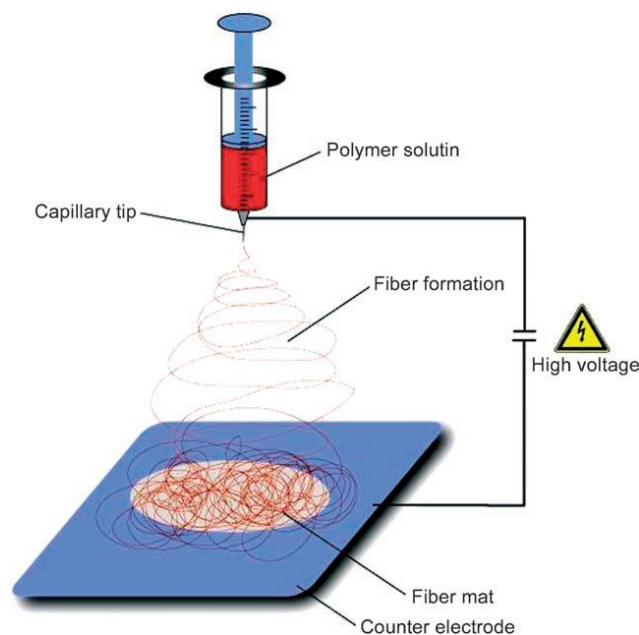


**Figure 2.4 :** Schematic diagram of the electrospinning setup [14].

In the electrospinning process, a polymer solution or melt is pumped through a spinneret and then a charged polymer solution is accelerated towards the grounded collector in a strong electrostatic field with applied voltage. The following causes the droplet, emerging from the spinneret end, to undergo deformation into a conical shape usually called the “Taylor cone”. This shape assumed as interact of the surface tension of the solution, the electric charges developed in the solution and the electrostatic force acting on it. When the applied voltage is reached to critical value at which the electrostatic force has overcome the surface tension of the solution, a fine jet of the solution occurs. The jet, after initial straight part, undergoes bending instability and a whipping motion due to the charge-charge repulsion between the spinneret and grounded collector. During this action, the solvent evaporates and the dry fibers deposit onto the collector [13, 15, 16].

There is developed and adopted method to produce bicomponent shell/core or hollow nanofiber structure called coaxial electrospinning. In this system a modification is made in the spinneret by inserting a smaller (inner) nozzle that fits concentrically inside the bigger (outer) nozzle to make a coaxial configuration. Figure 2.5 shows the schematic diagram of the coaxial electrospinning setup.

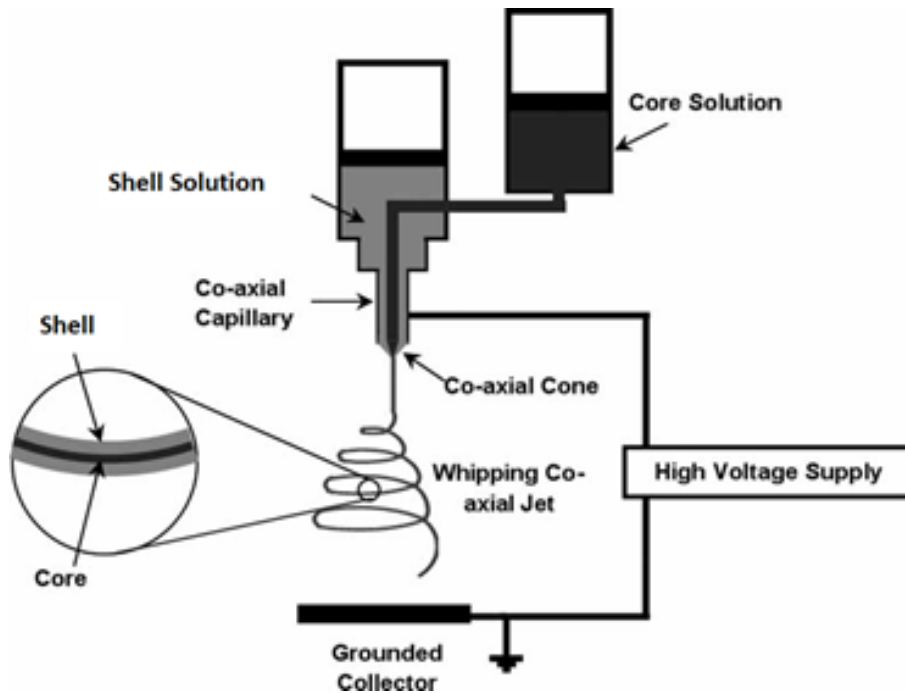


**Figure 2.5 :** Schematic diagram of the coaxial electrospinning setup [15].

The process of coaxial electrospinning is practically similar to that of the single jet electrospinning. In the coaxial electrospinning process, with applied voltage firstly the drop of shell solution at the tip displays cone-shaped deformation, then elongates and stretches owing to repulsion forces and increased applied voltage cause a fine jet extends from the cone. The core solution deforms subsequently into the conical shape due to the shearing of it with generated stresses in the shell solution, thus coaxial jet occurs at the tip of the cones. The shell/core nanofibers deposited at the collector when the jet undergoes bending instability and displays whipping motion, while the two solvents evaporate and leave dry nanofibers [15].

There are three group of parameters which are material, process and ambient that having strong effect on electrospinning process [15]. The Table 2.2 shows classification of these parameters. Figure 2.6a and 2.6b indicates the effect of solution parameters and process parameters on electrospinning process, respectively.

**Table 2.2 :** The parameters that effect the electrospinning process [15].

Electrospinning Type	Solution Parameters	Process Parameters	Ambient Parameters
Single Jet	Concentration Molecular Weight Viscosity Surface Tension Conductivity	Applied voltage Solution flow rates Tip to collector distance	Temperature Humidity
Coaxial	Solution viscosities Solution concentraiton Solvent/Solution miscibility and incompability Solvent vapor pressure Solution conductivities	Applied voltage Solution flow rates Tip to collector distance	Temperature Humidity

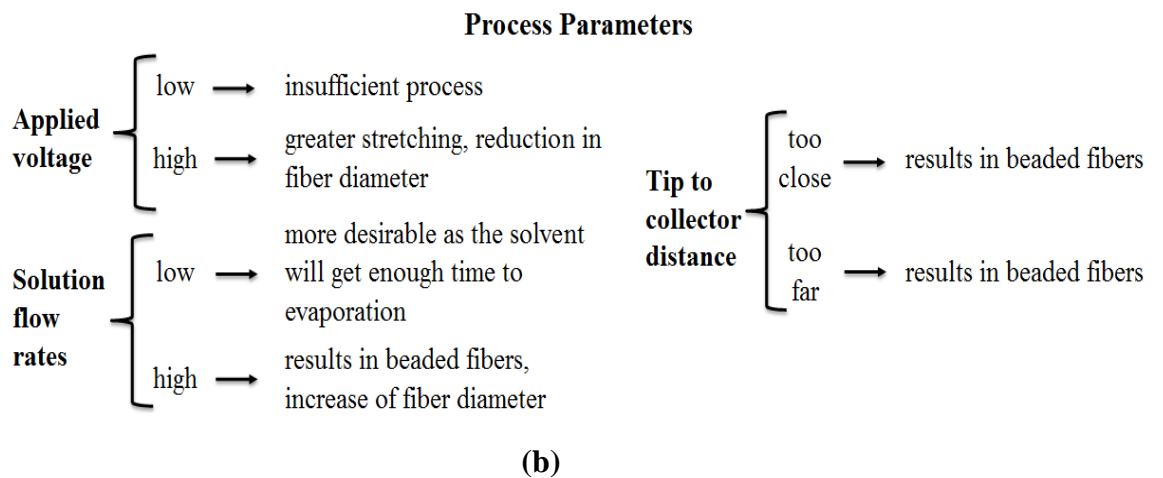
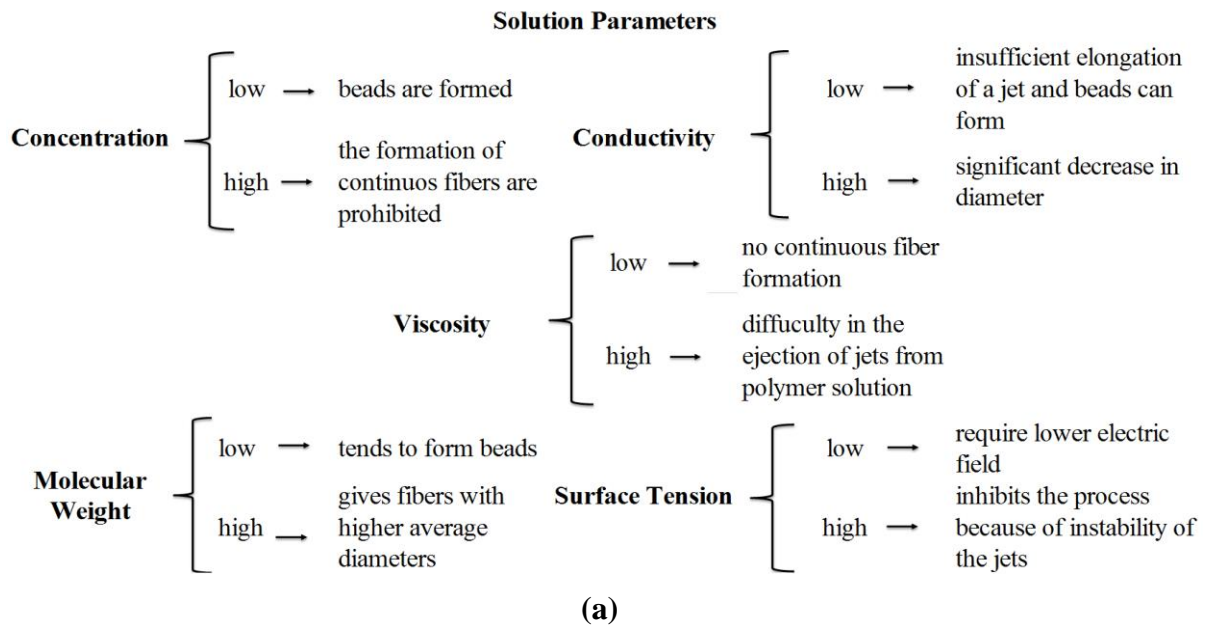


**Figure 2.6 :** Effect of parameters on electrospinning process: (a) Solution parameters. (b) Process parameters.

In other respects, in coaxial electrospinning experiment important material parameters are solution viscosities, solution concentration, solvent/solution miscibility and incompatibility, solvent vapor pressure and solution conductivities. Applied voltage, tip to collector distance and solution flow rates are important parameters as a process parameter, ambient and humidity important as regard of ambient parameters. Because of using two type of polymer solution, arrangement of these parameters plays an important role to form the composite nanofiber in this process. All these parameters should be selected as the optimum and require fine tuning to achieve desired nanowebs [15, 17, 18]. To summarize important parameters in consideration of coaxial electrospinning;

- ✓ shell solution should be electrospinnable itself,
- ✓ higher shell solution viscosity should be used,
- ✓ there should be low interfacial tension between the shell and the core solutions,
- ✓ used solvents should have low vapor pressure
- ✓ conductivity of shell solution should be higher,
- ✓ the core flow rate should generally lower [15].

On the other hand, each polymer-solvent system require distinctive parameter settings and there is just a narrow range for each applied parameter to produce proper nanoweb [15].

## **2.2.2 The use of PAN in electrospinning**

### **2.2.2.1 Polyacrylonitrile (PAN)**

Acrylonitrile (AN) is the monomer of poly(acrylonitrile) (PAN) polymer and its representative molecular formula is  $C_3H_3N$  [19]. Acrylonitrile very widely used in the manufacture of synthetic fibers, resins, plastics, elastomers and rubber over many years and used in the consumer products like textiles, drinking cups, automotive part and appliances [20]. In textile industry, PAN is very widely used as the raw material of acrylic fiber that improved and marketed by DuPont as a name of Orlon in 1941. Acrylic fibers are used in cloths like sweater, vest, jacket, socks, underwear and



sportswear, in home textile products like upholstery, carpet and blanket, also it is used in industrial technical textile products such as tarpaulins, sun blind, boat covers, reinforcing fillings in construction. Acrylic fibers are well-known for their very good thermal stability, high tensile strength and elastic modulus, low density, high moisture management and excellent thermal insulation properties. These superior features make PAN potential material to use in various applications. PAN can also be processed into ultrafine fibers via electrospinning and studies are quite new in this area [21, 22]. Thus, their usage in nanofiber production is promising for the some end uses like tissue engineering, sensor applications, composites, battery separators etc.

#### **2.2.2.2 PAN applications by electrospinning**

Conducts studies on production of polyacrylonitrile nanofibers by electrospinning method is fairly new. The one of the studies aims to investigate the individual and interactive effect of material and process parameters on diameter of produced PAN nanofibers with using different solution concentrations, applied voltage and collector distance. It is found that, effect of applied voltage in micron-scale fiber diameter was observed to be almost negligible when solution concentration and collector distance were high. However, all three factors were found statistically significant in the production of nano-scale fibers. The suggested parameter ranges for achievable lowest diameter distribution were; 8-10 wt% PAN solution in dimethylformamide (DMF), 12-16 kV applied voltage and 8 cm collector distance according the study [22]. In another study, PAN nanofibers were produced using 8-11 wt% PAN in DMF, 10-12 kV applied voltage and 20 cm collector distance. The desired diameters of PAN nanofibers were achieved by changing applied voltage and solution concentration and then effect of single fiber diameter on strength, modulus and toughness were investigated. The measured value of the highest strength and modulus of PAN nanofibers was found 5 to 10 times higher than commercial ultra-high molecular weight PAN microfibers [23]. In one study, PAN nanofibers were prepared by electrospinning method and the effect of polymer concentration on the morphology of nanofibers was studied. In production of nanofibers,  $1.5 \text{ kV}\cdot\text{cm}^{-1}$  of electric field,  $1.0 \text{ ml}\cdot\text{h}^{-1}$  flow rate and 15 cm collector distance were used as a constant parameters and polymer concentrations were varied from 2 w/v% to 7w/v%. It is observed that, the beads or beads on string structures were formed with dilute PAN solutions (2%, 3%,

4%) whereas homogeneous electrospun fibers were produced from semi-dilute solutions (5%, 6%, 7%) [24].

### **2.2.3 PCM application via electrospinning**

The researches and studies about usage of electrospinning in production of PCM containing fibers and nanowebs are also quite new. The one of the studies, includes production of phase change nanofibers by coaxial electrospinning using *n*-octadecane and *n*-eicosane as a core materials and TiO<sub>2</sub>- PVP (Polyvinylpyrrolidone) composite as a shell material. The enthalpy value of resulted *n*-octadecane–PVP nanofibers and *n*-eicosane–PVP nanofibers were 114 kJ.kg<sup>-1</sup> at 27°C and 88 kJ.kg<sup>-1</sup> at 37°C, respectively [25]. Other study contains, production of PEG10000-CA (cellulose acetate) core-shell nanofibers via electrospinning method and the reached heat of fusion was 86 kJ.kg<sup>-1</sup> at 58°C with 70wt% of PEG content in the fibers. They were seen that resulted PEG/CA composite nanofibers were suitable and promising for using as phase change fibers in thermal energy storage and thermal management applications [26]. In another study, polyethyleneglycol (PEG)-polyvinylidene fluoride (PVDF) core-shell nanofibers were fabricated by coaxial electrospinning with using three different type of PEG say, PEG1000, PEG2000 and PEG4000, as core materials. The resulted PEG1000/PVDF, PEG2000/PVDF and PEG4000/PVDF composite nanofibers was demonstrated enthalpy ratio of  $\Delta H_{\text{PEG/PVDF}}/\Delta H_{\text{PEG}}$  as 23%, 25% and 27% respectively, at the same core feed rate [27].

### 3. MATERIAL AND METHODS

#### 3.1 Materials

In this study we aim to produce bicomponent nanowebs which have great heat storage capacity and stability between certain temperature ranges. Core and shell materials were used to produce bicomponent nanofibers by coaxial electrospinning method.

##### 3.1.1 Core materials

We preferred to use three different types of phase change material (PCM) say, polyethylene glycol (PEG), polyethylene glycol methyl ether (PEGME) and paraffin wax (*n*-alkane), as core materials. Two temperature regions were considered for the phase transitions of PCMs and their nanoweb applications that were cold and normal regions. Cold temperature region indicates the interval from -10°C to 18°C while normal temperature region indicates the interval from 18°C – 43°C. Therefore, PCMs were chosen so that their melting points were included by one of these two regions.

##### 3.1.1.1 Polyethylene glycols

PEGs are composed of linear dimethyl ether chains with hydroxyl ending groups, HO—CH<sub>2</sub>—(CH<sub>2</sub>—O—CH<sub>2</sub>)<sub>n</sub>—CH<sub>2</sub>—OH, and accordingly possess dual feature of water solubility and organic solubility. The general chemical formula of PEGs is given in Fig. 3.1. Four types of PEGs, say PEG400, PEG600, PEG1000 and PEG1500, were used as technical grade chemicals from Merck Co., as shown in Table 3.1. PEG400 were used to produce nanowebs for cold temperature region applications and others were used to produce nanowebs for normal temperature region applications.

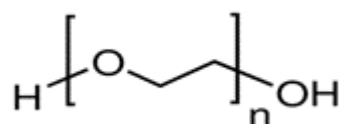


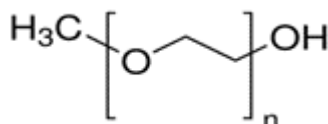
**Figure 3.1** : The general chemical formula of PEGs [19].

**Table 3.1 :** Characteristics of selected PEGs [28].

PEG	IUPAC Name	Molecular Formula	Average MW (g.mol <sup>-1</sup> )	Density (g.cm <sup>-3</sup> )	Melting Point (°C)	Solubility in Water	Application Region
PEG400	Poly(oxy ethylene)	C <sub>2n</sub> H <sub>4n+2</sub> O <sub>n+1</sub>	380-420	1.13	4–8	Soluble (20°C)	Cold
PEG600	Poly(oxy ethylene)	C <sub>2n</sub> H <sub>4n+2</sub> O <sub>n+1</sub>	570-630	1.13	17–22	Soluble (20°C)	Normal
PEG1000	Poly(oxy ethylene)	C <sub>2n</sub> H <sub>4n+2</sub> O <sub>n+1</sub>	950-1050	1.20	33–40	750 g.l <sup>-1</sup> (20°C)	Normal
PEG1500	Poly(oxy ethylene)	C <sub>2n</sub> H <sub>4n+2</sub> O <sub>n+1</sub>	1400-1600	1.20	44–48	500 g.l <sup>-1</sup> (20°C)	Normal

### 3.1.1.2 Polyethylene glycol methyl ethers

PEGME550 were preferred to produce nanoweb in cold temperature region and PEGME750 were preferred to produce nanoweb in normal temperature region and they were technical grade chemicals supplied from Sigma-Aldrich Inc. The general chemical formula of PEGMEs is given in Fig. 3.2 and characteristics of PEGMEs are shown in Table 3.2.

**Figure 3.2 :** The general chemical formula of PEGMEs [29].**Table 3.2 :** Characteristics of selected PEGMEs [29].

PEGME	IUPAC Name	Molecular Formula	Average MW (g.mol <sup>-1</sup> )	Density (g.cm <sup>-3</sup> )	Melting Point (°C)	Solubility in Water	Application Region
PEGME550	Methoxy poly(ethylene glycol)	C <sub>2n+1</sub> H <sub>4n+4</sub> O <sub>n+1</sub>	550	1.09	18-20	Soluble (20°C)	Cold
PEGME750	Methoxy poly(ethylene glycol)	C <sub>2n+1</sub> H <sub>4n+4</sub> O <sub>n+1</sub>	750	1.09	30	Soluble (20°C)	Normal

### 3.1.1.3 Paraffin waxes (*n*-alkanes)

The general chemical formula of *n*-alkanes is given in Figure 3.3. The five types of paraffin waxes, namely *n*-tetradecane, *n*-pentadecane, *n*-hexadecane, *n*-heptadecane and *n*-octadecane were preferred, two of them for cold temperature region applications and last three for normal temperature region applications. *n*-pentadecane supplied from Alfa Aesar, *n*-tetradecane supplied from Sigma-Aldrich Inc., *n*-hexadecane, *n*-heptadecane and *n*-octadecane supplied from Merck Co. and all were technical grade (See Table 3.3).



**Figure 3.3 :** The general chemical formula of paraffin wax (*n*-alkane) [29].

**Table 3.3 :** Characteristics of selected *n*-alkanes [28, 29, 30].

<i>n</i> -Alkane	IUPAC Name	Molecular Formula	Average MW (g.mol <sup>-1</sup> )	Density (g.mL <sup>-1</sup> )	Melting Point (°C)	Solubility in Water	Application Region
<i>n</i> -tetradecane	Tetradecane	C <sub>14</sub> H <sub>30</sub>	198.4	0.76	5.5	insoluble	Cold
<i>n</i> -pentadecane	Pentadecane	C <sub>15</sub> H <sub>32</sub>	212.4	0.77	10	insoluble	Cold
<i>n</i> -hexadecane	Hexadecane	C <sub>16</sub> H <sub>34</sub>	226.4	0.77	18	insoluble	Normal
<i>n</i> -heptadecane	Heptadecane	C <sub>17</sub> H <sub>36</sub>	240.5	0.78	22	insoluble	Normal
<i>n</i> -octadecane	Octadecane	C <sub>18</sub> H <sub>38</sub>	254.5	0.78	26–29	insoluble	Normal

### 3.1.2 Shell materials

#### 3.1.2.1 Supplied polymers

PAN copolymer which consists of 99.5% of Acrylonitrile (AN) and 0.5% of Maleic anhydride (MAH) was supplied from GoodFellow Corp. in powder form as a shell material to produce bicomponent nanofibers. Its average molecular weight is 150,000 g.mol<sup>-1</sup>, density is 1.18 g.cm<sup>-3</sup> and mean particle size is 50 micron [31]. The chemical formula of PAN is given in Fig. 3.4 and (C<sub>3</sub>H<sub>3</sub>N)<sub>n</sub> is the general representative formula for PAN.

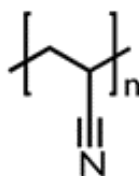


**Figure 3.4 :** The chemical formula of PAN [29].

#### 3.1.2.2 Synthesized polymers

We synthesized a type of grafted copolymer say PEG-MAH-g-PAN, with the aim of producing thermally and chemically stable hollow nanofibers, suitable for heat storage applications. Its recipe that we developed in the study and the detailed process steps are given in Section 3.2.1. *p*-Toluenesulfonic acid (PTSA), hexane, ethanol, diethyl ether, dimethylacetamide (DMAc), azobisisobutyronitrile (AIBN), maleic anhydride (MAH), PEG and acrylonitrile (AN) are the chemicals used in the synthesis process that all of them was technical grade and used without further purification. DMAc, hexane, diethyl ether, ethanol absolute, PEG and MAH supplied from Merck Co.;

PTSA, AIBN and AN supplied from Sigma-Aldrich Inc. The materials used in the synthesis, their characteristics and functions are indicated in the Table 3.4.

**Table 3.4 :** The materials used in the synthesis and their properties [28, 29, 30].

Material	IUPAC Name	Molecular Formula	Average MW (g.mol <sup>-1</sup> )	Density (g.cm <sup>-3</sup> )	Solubility in Water	Its Function
PTSA	4-methylbenzene sulfonic acid	CH <sub>3</sub> C <sub>6</sub> H <sub>4</sub> SO <sub>3</sub> H	199.22	1.24	67 g.100 mL <sup>-1</sup>	Catalyst
Hexane	Hexane	C <sub>6</sub> H <sub>14</sub>	86.18	0.65	9.5 mg.L <sup>-1</sup>	Precipitaion agent
Ethanol	Ethanol	C <sub>2</sub> H <sub>6</sub> O	46.07	0.79	1000000 mg.L <sup>-1</sup>	Precipitaion agent, Solvent
Diethyl ether	Ethoxyethane	C <sub>4</sub> H <sub>10</sub> O	74.12	0.71	69 g.L <sup>-1</sup>	Precipitaion agent
DMAc	<i>N,N</i> -Dimethylacetamide	C <sub>4</sub> H <sub>9</sub> NO	87.12	0.94	Miscible	Solvent
AIBN	2,2'-Azobis(2-methyl propionitrile)	C <sub>8</sub> H <sub>12</sub> N <sub>4</sub>	164.21	1.1	Insoluble	Initiator
MAH	Furan-2,5-dione	C <sub>4</sub> H <sub>2</sub> O <sub>3</sub>	98.06	1.48	Reacts	Esterification material
PEG	poly(oxyethylene)	C <sub>2n</sub> H <sub>4n+2</sub> O <sub>n+1</sub>	18.02 + (44.05n)	1.1	Soluble	Grafting material
AN	prop-2-enenitrile	C <sub>3</sub> H <sub>3</sub> N	53.06	0.8	7 g.100 mL <sup>-1</sup>	Backbone material for grafting

### 3.2 Experimental Study

#### 3.2.1 Polymer synthesis

Two subsequent reactions were performed in the synthesis. At first PEG-MAH esterification reaction was carried out; then, grafting PEG-MAH to poly(AN) backbone was performed, which resulted in PEG-MAH-g-PAN grafted copolymer. PEG1000 and PEG1500 were preferred for grafting PEG. Chemical formulae of MAH and PEG, and AN and Poly(AN) are shown in Figure 3.5 and Figure 3.6, respectively. The generalized reaction steps for both esterification and grafting are separately described below.



**Figure 3.5 :** Chemical formula of: (a) MAH. (b) PEG [29].



**Figure 3.6 :** Chemical formula of: (a) AN. (b) Poly(AN) [19].

The process steps for PEG-MAH esterification reaction are as follows:

1. 0.001 mol of PEG and absolute ethanol are put in a three-necked reaction flask and reflux setup is arranged,
2. Temperature is heated up to 60°C, then dissolution of PEG in absolute ethanol is provided under the inert atmosphere,
3. After dissolution of PEG, 0.001 mol MAH is added into the reaction flask and stirring is continued for 30 minutes at 60°C,
4. Subsequently, PTSA is added to the reaction flask as a catalyst,
5. Temperature is heated up to 90°C and the mixture is refluxed during 3 hours for the polymerization,
6. At the end of the time, the product is precipitated in diethyl ether and than is dried by keeping at room temperature overnight.

The chemical reaction and PEG-MAH product is shown in Figure 3.7.

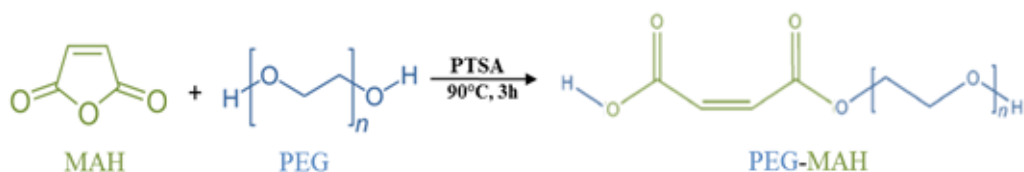


**Figure 3.7 :** Chemical reaction of PEG-MAH esterification [32].

The process steps for PEG-MAH-g-PAN reaction are as follows:

1. 5 g of PEG-MAH ester is dissolved in DMAc at 60°C,
2. 5 g of AN is added into a solution so that the weight ratio of PEG-MAH:AN is 1:1,
3. Inert gas is passed through the reaction flask and stirring is continued at the same temperature for 30 minutes,
4. At the end of time, AIBN is added to a reaction flask as a initiator,
5. Reaction is continued during 24 hours, at 70°C under inert atmosphere,
6. At the end of time, polymerized bulk is cooled down to room temperature and precipitated in 3:1 (by volume) ethanol:hexane solution,

7. The resulted precipitate is washed at least three times with ethanol:hexane solution thus unreacted reactans are removed,
8. The , the yielded end product is allowed to dry at room temperature.

At the end of these two subsequent reactions, firstly PEG1000-MAH and PEG1500-MAH esters were obtained and then grafting and polymerization of PEG1000-MAH-g-PAN and PEG1500-MAH-g-PAN were achieved. Figure 3.8 shows the chemical reaction and the product of PEG-MAH-g-PAN.

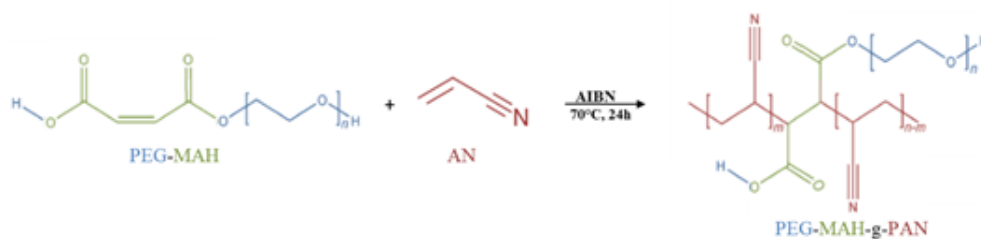


**Figure 3.8 :** Chemical reaction of the graft copolymer PEG-MAH-g-PAN [32].

### 3.2.2 Electrospinning process

With the aim of the manufacture of bicomponent nanowebs from PAN/PCM copolymers and hollow nanofibers from PEG-MAH-g-PAN grafted copolymer we performed coaxial electrospinning experiments, using Yflow<sup>®</sup> coaxial electrospinning device (Spain). Two different model of nanowebs were produced. One of them was PAN/PCM as a shell/core structure and the other one was PCM grafted PAN copolymer used as a shell to produce hollow nanofiber strucutre.

Yflow<sup>®</sup> coaxial electrospinning device suitable for the production of shell/core nanowebs in one-step. There are two coaxial needles connected to a high voltage power supply and two separate pump system for shell and core solution. The device is given in Figure 3.9.

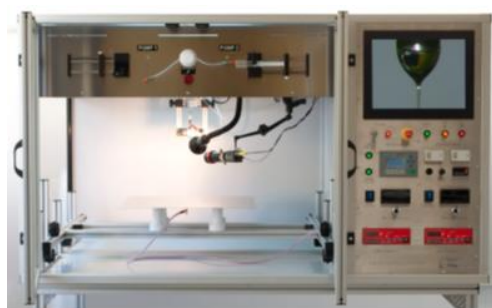


**Figure 3.9 :** YFlow<sup>®</sup> coaxial electrospinning device [33].



The coaxial injection system is composed of the stainless steel outer and inner nozzles. The outer nozzle had an outer diameter (OD) of 1.4 mm and an inner diameter (ID) of 0.9 mm, while the inner nozzle had OD and ID of 0.9 and 0.6 mm, respectively. Device has a grounded flat stainless steel collecting plate of 200x200 mm to collect the nanoweb. The distance between the nozzle and the collector can be adjustable between 15mm and 500mm.

In electrospinning experiments, the charged nanoparticles are able to escape from electric field during their travel from the emitter to the collector and due to their nanometric dimension, they can be easily dragged by air flows. Yflow<sup>®</sup> device has double polarized system (-30 kV, +30kV) thus the fly out of nanoparticles from the electric field greatly reduced and electrospinning performance is improved. Figure 3.10 shows the differences of simple and double polarized system.

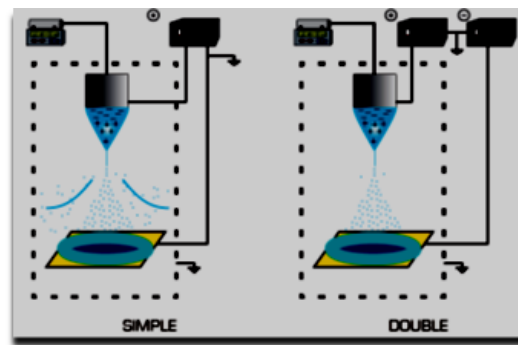


**Figure 3.10 :** Schematic of simple and double polarized systems [33].

The Taylor cone is very important parameter that, in order to get a steady electrospinning process, Taylor cone steadiness is required. Thus, its visualization is crucial for checking the performance of the process. With Taylor cone visualization system in device we were able to follow the process easily, Figure 3.11 shows this property.



**Figure 3.11 :** The Taylor cone visualization system [33].

Beside these features, device has microstepping pumps allow precise flow rate control to obtain high quality nanoweb. Figure 3.12 shows the coaxial electrospinning design and method schematically.

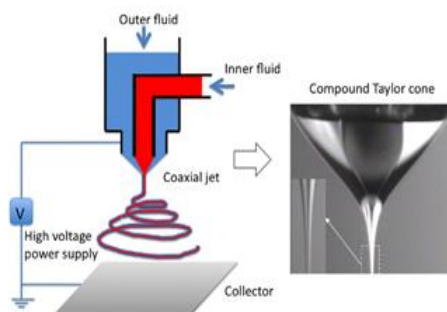


**Figure 3.12** : Schematic of coaxial design [34].

After several trials and fine tuning, the nanoweb produced according to the parameters specified. Besides these parameters, different concentrations selected for both core and shell solutions after several trials. Two different concentrations which were 4wt% and 6wt% of PAN in DMAc used as a shell material. The concentrations of the core solutions was decided according to their features. 40wt% and 30wt% solutions of PEG in DMAc, 30wt% and 20wt% solutions of PEGME in DMAc, lastly 50wt% solutions of solid *n*-alkanes in hexane and 100wt% (pure) solutions of liquid *n*-alkanes were used as a core solutions. The electrospinning parameters for each produced nanoweb is given in Table 3.5.

**Table 3.5** : The used parameters in the electrospinning process of shell/core nanoweb.

Shell	Shell Concentration (wt%)	Core	Core Concentration (wt%)	Shell Flow Rate (mL/h)	Core Flow Rate (mL/h)	Injector Voltage (kV)	Collector Voltage (kV)	Tip to Collector Distance (cm)	Sample Code
PAN	4	-	-	0.03	-	8.38	-7.00	15	4S
PAN	6	-	-	0.03	-	7.00	-7.00	15	6S
PAN	4	PEG400 + PEG1000	40 + 1	0.06	0.01	6.20	-6.10	15	4S40CPEG1 (A1)
PAN	4	PEG400 + PEG1500	40 + 1	0.07	0.02	6.20	-6.10	15	4S40CPEG2 (A2)
PAN	4	PEG600 + PEG1000	40 + 1	0.06	0.02	6.20	-6.10	15	4S40CPEG3 (A3)
PAN	4	PEG600 + PEG1500	40 + 1	0.06	0.02	6.20	-6.10	15	4S40CPEG4 (A4)
PAN	4	PEG1000	40	0.05	0.01	6.35	-6.17	15	4S40CPEG5 (A5)
PAN	4	PEG1500	40	0.06	0.02	6.35	-6.33	15	4S40CPEG6 (A6)
PAN	4	PEG400 + PEG1000	30 + 1	0.07	0.02	6.20	-6.10	15	4S30CPEG7 (A7)
PAN	4	PEG400 + PEG1500	30 + 1	0.06	0.01	6.20	-6.20	15	4S30CPEG8 (A8)

**Table 3.5 (continued) :** The used parameters in the electrospinning process of shell/core nanowebs.

Shell	Shell Concentration (wt%)	Core	Core Concentration (wt%)	Shell Flow Rate (mL/h)	Core Flow Rate (mL/h)	Injector Voltage (kV)	Collector Voltage (kV)	Tip to Collector Distance (cm)	Sample Code
PAN	4	PEG600 + PEG1000	30 + 1	0.06	0.01	8.22	-8.00	15	4S30CPEG9 (A9)
PAN	4	PEG600 + PEG1500	30 + 1	0.04	0.01	6.50	-6.50	15	4S30CPEG10 (A10)
PAN	4	PEG1000	30	0.04	0.01	6.60	-6.50	15	4S30CPEG11 (A11)
PAN	4	PEG1500	30	0.04	0.01	6.00	-6.00	15	4S30CPEG12 (A12)
PAN	6	PEG400 + PEG1000	40 + 1	0.05	0.01	6.50	-6.50	15	6S40CPEG13 (A13)
PAN	6	PEG400 + PEG1500	40 + 1	0.06	0.01	6.20	-6.00	15	6S40CPEG14 (A14)
PAN	6	PEG600 + PEG1000	40 + 1	0.05	0.01	6.50	-6.50	15	6S40CPEG15 (A15)
PAN	6	PEG600 + PEG1500	40 + 1	0.05	0.01	6.50	-6.50	15	6S40CPEG16 (A16)
PAN	6	PEG1000	40	0.04	0.01	6.00	-6.00	15	6S40CPEG17 (A17)
PAN	6	PEG1500	40	0.02	0.01	6.27	-6.08	15	6S40CPEG18 (A18)
PAN	6	PEG400 + PEG1000	30 + 1	0.04	0.01	6.35	-6.35	15	6S30CPEG19 (A19)
PAN	6	PEG400 + PEG1500	30 + 1	0.04	0.01	6.65	-6.65	15	6S30CPEG20 (A20)
PAN	6	PEG600 + PEG1000	30 + 1	0.04	0.01	6.20	-6.10	15	6S30CPEG21 (A21)
PAN	6	PEG600 + PEG1500	30 + 1	0.04	0.01	6.10	-6.00	15	6S30CPEG22 (A22)
PAN	6	PEG1000	30	0.04	0.01	6.50	-6.50	15	6S30CPEG23 (A23)
PAN	6	PEG1500	30	0.04	0.01	6.10	-6.00	15	6S30CPEG24 (A24)
PAN	4	PEGME 550	30	0.04	0.01	6.60	-6.60	15	4S30CPEGME1 (B1)
PAN	4	PEGME 750	30	0.04	0.01	6.75	-6.50	15	4S30CPEGME2 (B2)
PAN	4	PEGME 550	20	0.04	0.01	6.90	-6.90	15	4S20CPEGME3 (B3)
PAN	4	PEGME 750	20	0.03	0.02	8.00	-8.00	15	4S20CPEGME4 (B4)
PAN	6	PEGME 550	30	0.04	0.02	6.50	-6.90	15	6S30CPEGME5 (B5)
PAN	6	PEGME 750	30	0.04	0.02	7.10	-6.75	15	6S30CPEGME6 (B6)
PAN	6	PEGME 550	20	0.04	0.02	7.00	-7.00	15	6S20CPEGME7 (B7)
PAN	6	PEGME 750	20	0.05	0.04	8.00	-7.55	15	6S20CPEGME8 (B8)
PAN	6	Tetradecane (C <sub>14</sub> H <sub>30</sub> )	100	0.02	0.0006	6.76	-6.00	15	6S100CPW1 (C1)
PAN	6	Pentadecane (C <sub>15</sub> H <sub>32</sub> )	100	0.02	0.015	7.00	-7.00	15	6S100CPW2 (C2)
PAN	6	Hexadecane (C <sub>16</sub> H <sub>34</sub> )	100	0.02	0.009	6.51	-4.95	15	6S100CPW3 (C3)
PAN	6	Heptadecane (C <sub>17</sub> H <sub>36</sub> )	100	0.02	0.01	6.00	-6.00	15	6S100CPW4 (C4)
PAN	6	Octadecane (C <sub>18</sub> H <sub>38</sub> )	50	0.02	0.01	6.00	-6.00	15	6S50CPW5 (C5)

On the other hand, for the production of hollow nanofibers, the coaxial electrospinning was also performed using only a shell solution. To prepare the shell solution, 6wt% PAN (dissolved in dimethylacetamide) and 10wt% synthesized grafted copolymer (dissolved in dimethylacetamide), either PEG1000-MAH-g-PAN or PEG1500-MAH-g-PAN, were mixed at a ratio of 1:1 in a magnetic stirrer at a room temperature. The prepared mixture of the shell material was then pumped into the

injection nozzle without a core solution, Table 3.6 shows the used electrospinning parameters.

**Table 3.6 :** The used parameters in the electrospinning process of hollow nanofibers.

Shell	Shell to Shell Concentration (wt%)	Core	Shell Flow Rate (mL/h)	Core Flow Rate (mL/h)	Injector Voltage (kV)	Collector Voltage (kV)	Tip to Collector Distance (cm)	Sample Code
PAN + PEG1000-MAH-g-PAN	50 (6%) : 50 (10%)	-	0.04	-	10.00	-8.50	15	D1
PAN + PEG1500-MAH-g-PAN	50 (6%) : 50 (10%)	-	0.04	-	10.00	-9.00	15	D2

### 3.3 Characterization

#### 3.3.1 Structural analysis

##### 3.3.1.1 Fourier transform infrared spectroscopy (FTIR)

In FTIR technique IR radiation is passed through a sample that some of the infrared radiation is absorbed by the sample and some of it is passed through (transmitted). The resulting spectrum represents the molecular absorption and transmission, creating a molecular fingerprint of the sample. An infrared spectrum represents a fingerprint of a sample with absorption peaks which correspond to the frequencies of vibrations between the bonds of the atoms making up the material. Because each different material is a unique combination of atoms, no two compounds produce the exact same infrared spectrum. [35].

FTIR analyses were done with PerkinElmer's Spectrum Two IR Spectrometer. FTIR analysis were recorded in the range of 4000-650  $\text{cm}^{-1}$  at a resolution of 4  $\text{cm}^{-1}$  for all samples and after four consecutive measurements the average of them was taken as a result.

##### 3.3.1.2 Nuclear magnetic resonance spectrometry (NMR)

Nuclei of atoms imagined that they are spinning on their axis and each of them have a characteristic spin. The NMR spectroscopy is based on this phenomena that these magnetic properties of them can give some chemical information about sample [36, 37].

NMR analysis were performed with Bruker 300 MHz Liquid State NMR machine in the Middle East Technical University Central Laboratory. Proton ( $^1\text{H}$ ) and carbon-13 ( $^{13}\text{C}$ ) analysis were conducted in NMR. Prior to the experiment, samples are prepared by dissolving in deuterated solvents. For  $^1\text{H}$ NMR 10 mg sample, for  $^{13}\text{C}$ NMR 40 mg sample are dissolved in 1 mL deuterated solvent. Samples should be dissolved homogenously. After preparation, sample tube is placed into machine than shim setting is done and both  $^1\text{H}$  and  $^{13}\text{C}$  measurement is performed separately based on one measurement. Afterward, results are converted into spectrums. Analysis are conducted between 0-16 ppm for  $^1\text{H}$  and, between 0-200 ppm for  $^{13}\text{C}$ .

### **3.3.1.3 Scanning electron microscope (SEM)**

A SEM include focused electron beam that when these electrons and sample are interacts an image is obtain which give information about surface topogrfay and composition of sample [38]. In addition, it is one of the method to see the fibers in nanoscale significantly.

SEM analyses were peformed with a JEOL JXA 840A type instrument in Yıldız Technical University Central Laboratory. To prepare the SEM samples, dried nanowebbs were placed on standard mounts, 15 mm in diameter and 2 mm in depth, under vacuum and coated with a 1-2 nm thick conductive layer of gold to prevent charging during imaging. Fiber diameter distribution analyses of the SEM images of nanoweb samples were performed using “ImageJ-DiameterJ” software [39, 40].

### **3.3.2 Thermal analysis**

#### **3.3.2.1 Differantial scanning calorimetry (DSC)**

Differantial scanning calorimetry (DSC) is a thermal analysis technique that looks at how material's heat capacity ( $C_p$ ) is changed by temperature. A sample of known mass is either heated or cooled and the changes in its heat capacity are tracked as changes in the heat flow. This allows the detection of transitions such as melts, glass transitions, phase changes, and curing. Because of this flexibility, since most materials exhibit some sort of transitions [41].

Heat capacity ( $C_p$ ) is the amount of heat required to raise a unit mass of a material one degree in temperature (3.1).

$$Cp = Q \div (\Delta T \times m) \quad (3.1)$$

In the formula (3.1), Cp = specific heat, Q = heat added, m = mass of material,  $\Delta T$  = change in temperature.

The thermal analyses of samples were performed with DSC4000 machine which is product of PerkinElmer as illustrated in Figure 3.13.



**Figure 3.13 :** PerkinElmer DSC4000 machine.

The generalized applied method steps are as follows;

1. Hold for 1 min at  $T_{\text{start}}$ ,
2. Heat from  $T_{\text{start}}$  to  $T_{\text{end}}$  at  $10.00^{\circ}\text{C}\cdot\text{min}^{-1}$ ,
3. Hold for 1 min at  $T_{\text{end}}$ ,
4. Cool from  $T_{\text{end}}$  to  $T_{\text{start}}$  at  $10.00^{\circ}\text{C}\cdot\text{min}^{-1}$ ,
5. Hold for 1 min at  $T_{\text{start}}$ .

$T_{\text{start}}$  and  $T_{\text{end}}$  are selected separately for all samples depending on their melting point ( $T_g$ ) which  $T_{\text{start}}$  is approximately  $T_g - (30 \text{ or } 40^{\circ}\text{C})$ ,  $T_{\text{end}}$  is approximately  $T_g + (30 \text{ or } 40^{\circ}\text{C})$ .

In DSC analysis of all PCMs used as core, PAN copolymer and synthesized copolymers these 5 steps were repeated for 10 times that means that sample was heated 10 times than cooled 10 times, totally 10 heating-cooling cycles were applied. For nanowebs these 5 steps were repeated for 4 times that means sample was heated 4 times than cooled 4 times, totally 4 heating-cooling cycles were applied.

### **3.3.3 Characterization of solutions used in electrospinning**

#### **3.3.3.1 Electrical conductivity analysis**

The electrical conductivity measurements were performed using Mettler Toledo S80 Multi Conductometer. All core and shell solutions were conducted with prob 741, which suitable for measurement range of 0.001–500  $\mu\text{S}\cdot\text{cm}^{-1}$ . Prior to experiment calibration is performed with 84  $\mu\text{S}\cdot\text{cm}^{-1}$  standart solution and cell constant was  $\leq 0.1$  in all measurements.

#### **3.3.3.2 Viscosity analysis**

The dynamic viscosity measurements of all shell and core solutions were conducted using SNB-1 model Stepless Speed Regulation Rotary Display Viscometer. The instrument was designed and manufactured with four rotors (No.1, No.2, No.3, No.4) and four different velocity (6 rpm, 12 rpm, 30 rpm, 60 rpm), which enable it to measure any viscosity value between 1 to 100000 mPa.s. In order to perform measuring viscosity of solution, first you should estimate the viscous range of the sample to be measured and then choose the little dimensioned rotor and the slow rotating speed as per the sample with high viscosity and choose the large dimensioned rotor as per the sample with low viscosity. If the mark of the percentage meter between 20% - 90% the measured value is in normal range, if the value is not beyond this limit, the viscosity meter will alarm that means you should change the rotating speed and rotor [42, 43].





## 4. RESULTS

### 4.1 Characteristics of Shell and Core Solutions

Results of viscosity and electrical conductivity measurements are given in Table 4.1.

**Table 4.1 :** Viscosity and conductivity results of shell and core solutions.

Solutions	Solvent	Viscosity (Pa.s)	Conductivity ( $\mu\text{S.cm}^{-1}$ )
6wt% PAN	DMAc	0.533	19.4
4wt% PAN	DMAc	0.182	15.3
40wt% PEG400 +1%PEG1000	DMAc	0.013	30.4
30wt% PEG400 +1%PEG1000	DMAc	0.010	45.3
40wt% PEG400 +1%PEG1500	DMAc	0.012	35.6
30wt% PEG400 +1%PEG1500	DMAc	0.009	52.4
40wt% PEG600 +1%PEG1000	DMAc	0.016	19.7
30wt% PEG600 +1%PEG1000	DMAc	0.010	28.1
40wt% PEG600 +1%PEG1500	DMAc	0.016	20.9
30wt% PEG600 +1%PEG1500	DMAc	0.010	25.5
40wt% PEG1000	DMAc	0.014	13.8
30wt% PEG1000	DMAc	0.012	15.6
40wt% PEG1500	DMAc	0.016	31.2
30wt% PEG1500	DMAc	0.011	24.6
30wt% PEGME550	DMAc	0.003	0.9
20wt% PEGME550	DMAc	0.002	0.8
30wt% PEGME750	DMAc	0.003	1.5
20wt% PEGME750	DMAc	0.002	1.4
100wt% Tetradecane	-	0.002	0.0
100wt% Pentadecane	-	0.003	0.0
100wt% Hexadecane	-	0.004	0.0
100wt% Heptadecane	-	0.005	0.0
50wt% Octadecane	Hexane	0.001	0.0

The viscosity values and the corresponding conductivities of both core and shell solutions are given in the Table 4.1 were obtained suitable to attain the optimum electrospinning conditions in the manufacture of the nanowebs. The viscosities of the solutions showed increases with the increase in concentrations. The conductivities for PAN and PEGME solutions showed increases, conductivities of PEG solutions showed decreases with the increase in concentrations.

## 4.2 Structural Analysis Results

### 4.2.1 Nuclear magnetic resonance spectrometry (NMR) results of synthesized copolymers

$^1\text{H}$ NMR and  $^{13}\text{C}$ NMR analysis results are given respectively in Figure 4.1 and 4.2 for the synthesized copolymers, say PEG1000-MAH-g-PAN and PEG1500-MAH-g-PAN.

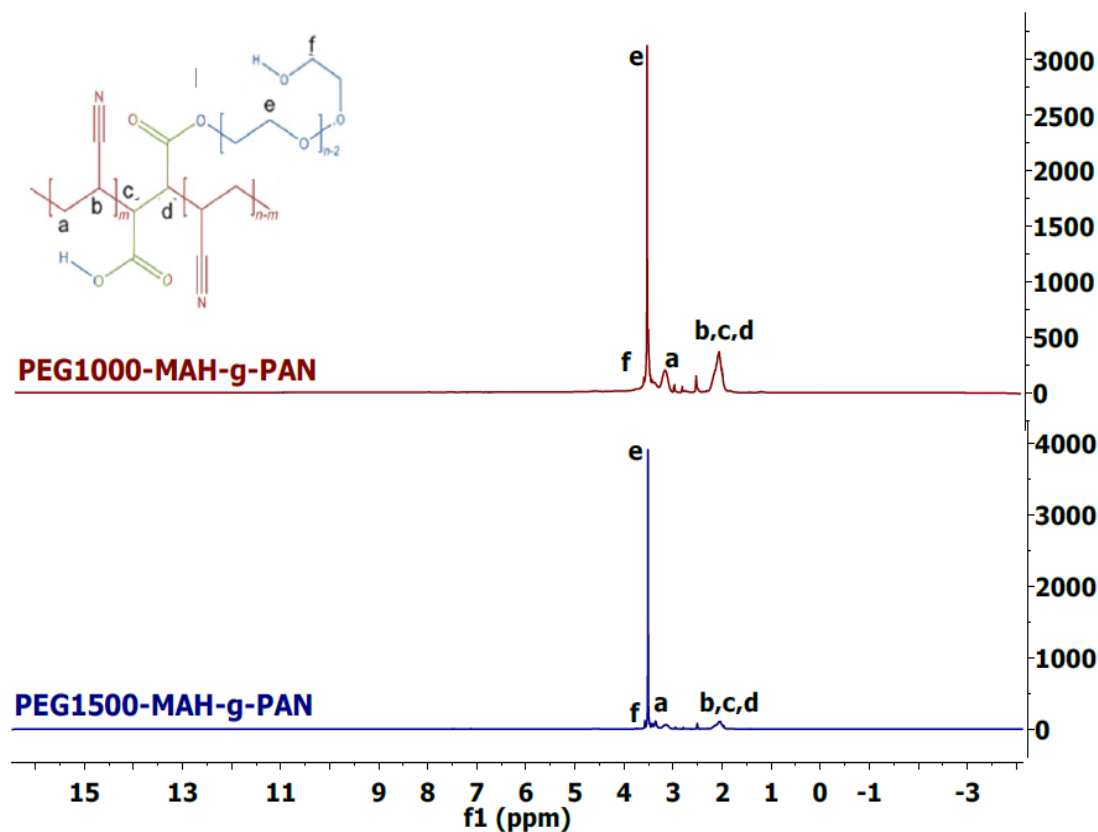


**Figure 4.1 :**  $^1\text{H}$ NMR graphs of synthesized PEG1000-MAH-g-PAN and PEG1500-MAH-g-PAN copolymers.

The  $^1\text{H}$ NMR spectra of two samples are alike. The H signals between 2.0-3.0 ppm (labeled a, b, c, d) belong to the alkyl protons of PAN backbone. The H signals around 3.5 ppm (labeled e) correspond to the alkyl protons of grafted PEG. The alkyl protons of PEG are appeared at around 4.6 ppm. The appearance of peaks between 3.0-3.5 ppm and disappeared peaks around 6.0 ppm indicate that grafting of PEG-MAH to PAN backbone is achieved for both two copolymers.

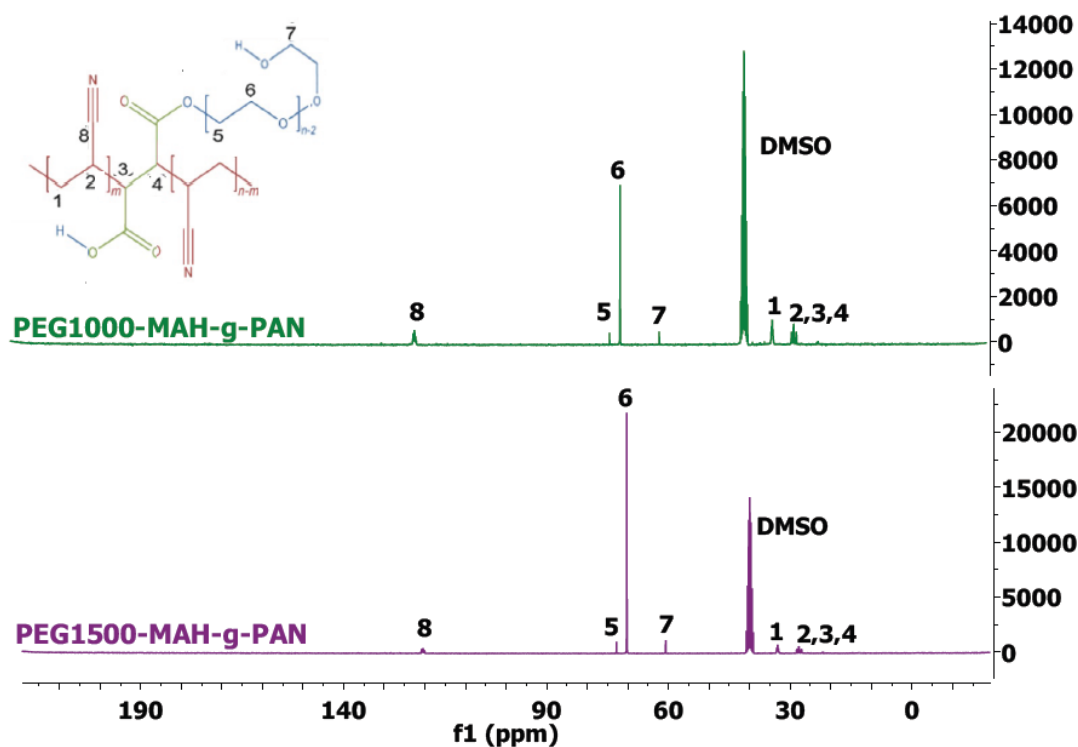


**Figure 4.2 :**  $^{13}\text{C}$ NMR graphs of synthesized PEG1000-MAH-g-PAN and PEG1500-MAH-g-PAN copolymers.

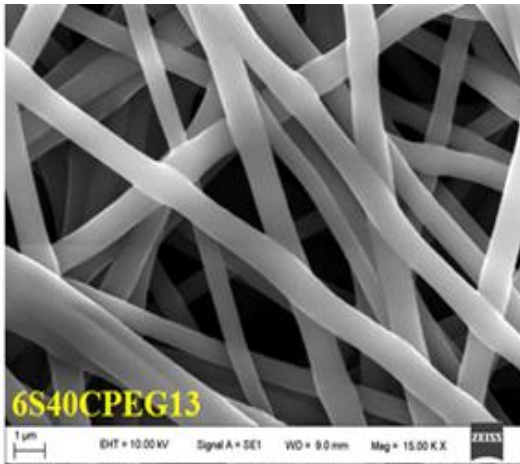
The  $^{13}\text{C}$ NMR spectra of two samples are alike. The signals of C between 26-29 ppm belong to the  $-\text{CH}$  groups of PAN backbone (labeled 2) and  $\text{CH}_2-\text{CH}$  bonds of MAH (labeled 3, 4). The peaks appeared between 31-34 ppm indicate  $-\text{CH}_2$  groups of PAN (labeled 1). The signals at 60 ppm correspond to the C atoms of  $\text{CH}_2-\text{CH}$  bonds. The C signals at 70-71 ppm belong to the  $\text{CH}_2\text{O}$  bonds of PEG and signals around 120 ppm correspond to the  $-\text{C}\equiv\text{N}$  bonds of PAN backbones.  $^1\text{H}$ NMR and  $^{13}\text{C}$ NMR results are in good agreement with FTIR results, suggesting that the synthesis of PEG-MAH-g-PAN were performed successfully.

#### 4.2.2 Scanning electron microscope (SEM) results of produced nanowebs

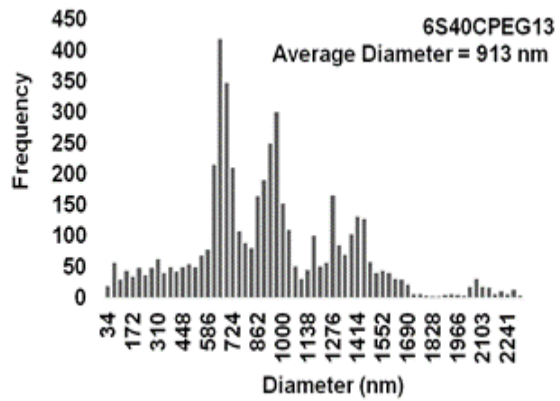
SEM analysis was performed for all produced nanowebs and diameter distribution analysis was conducted based on SEM images with 15000 K X magnification.

##### 4.2.2.1 SEM of PAN/PEG nanowebs

SEM images and related diameter distribution analysis of PAN/PEG nanowebs are given as four selected samples in Figure 4.3, 4.4, 4.5 and 4.6.

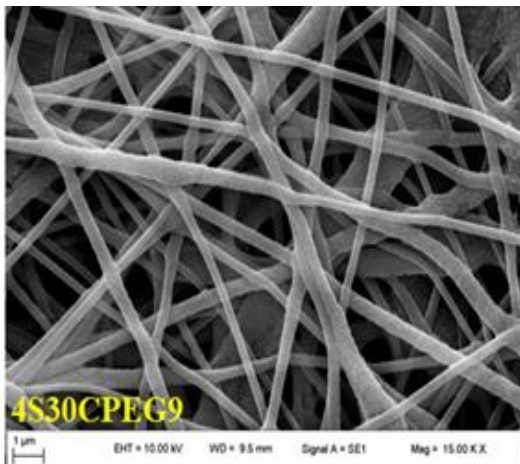


(a)

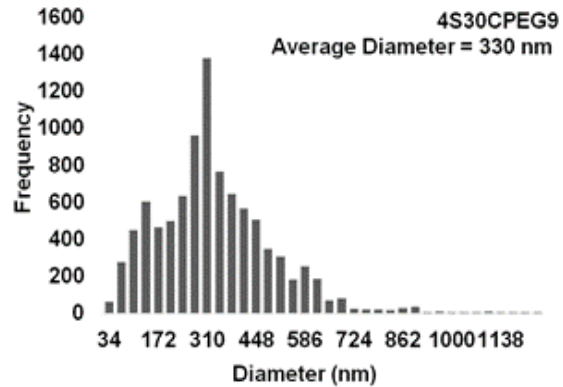


(b)

**Figure 4.3 :** (a) SEM image of 6S40CPEG13 nanoweb. (b) Diameter distribution histogram of 6S40CPEG13 nanoweb.

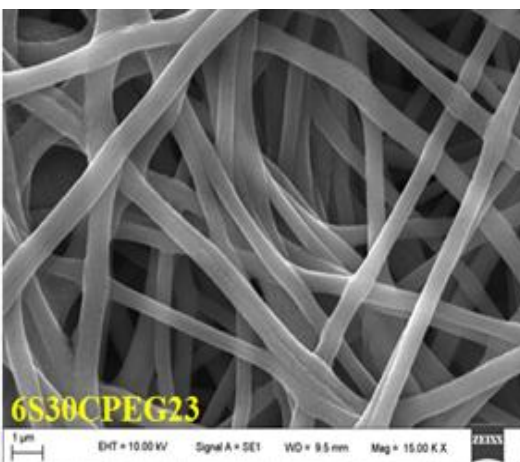


(a)

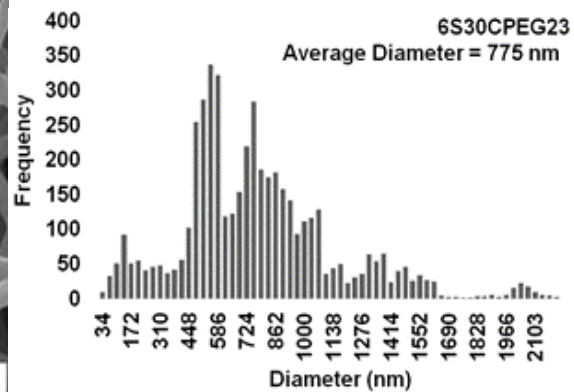


(b)

**Figure 4.4 :** (a) SEM image of 4S30CPEG9 nanoweb. (b) Diameter distribution histogram of 4S30CPEG9 nanoweb.



(a)



(b)

**Figure 4.5 :** (a) SEM image of 6S30CPEG23 nanoweb. (b) Diameter distribution histogram of 6S30CPEG23 nanoweb.

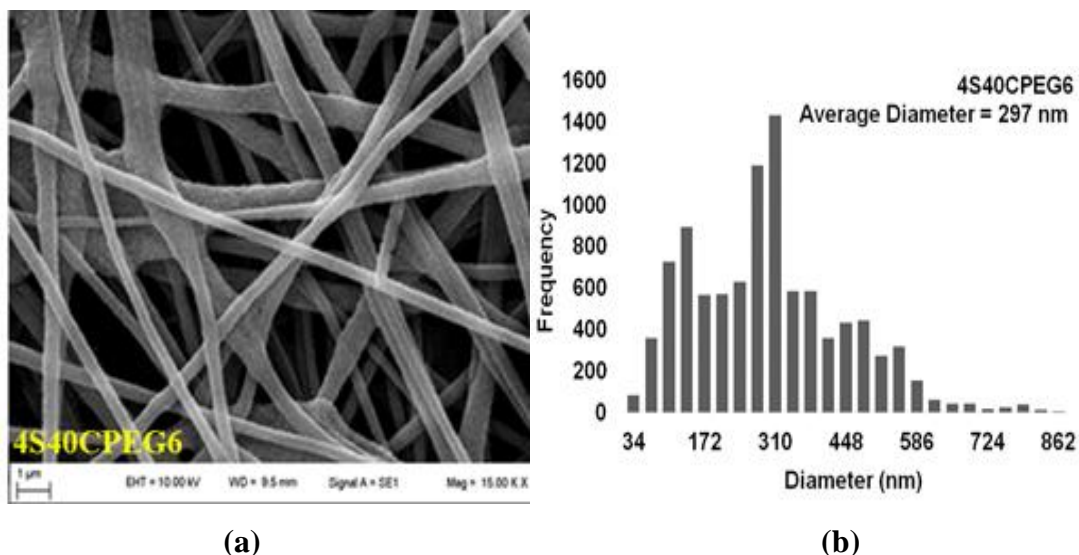


**Figure 4.6 :** (a) SEM image of 4S40CPEG6 nanoweb. (b) Diameter distribution histogram of 4S40CPEG6 nanoweb.

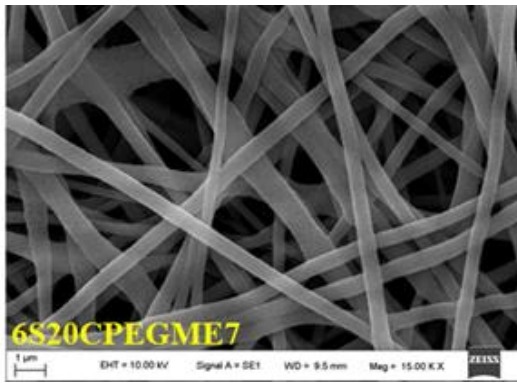
SEM images of PAN/PEG nanowebs shown in Figures 4.3, 4.4, 4.5 and 4.6 displayed generally beadless, smooth and cylindrical nanofibers. The rest of nanowebs composed of PAN/PEG shell/core combination also gave similar properties.

According to the results of diameter analyses the mean diameter values of nanofibers for PAN/PEG nanowebs ranged from 280 nm to 913 nm. Nanofiber diameter distributions of four samples centered around 280-300 nm, say 4S40CPEG6 (A6), 4S30CPEG10 (A10), 4S30CPEG11 (A11) and 4S30CPEG12 (A12); the distributions of six nanowebs centered around 301-500 nm, say 4S40CPEG1 (A1), 4S40CPEG3 (A3), 4S40CPEG5 (A5), 4S30CPEG8 (A8), 4S30CPEG9 (A9) and 6S30CPEG24 (A24) and rest of them centered in a range from 501 nm-913 nm.

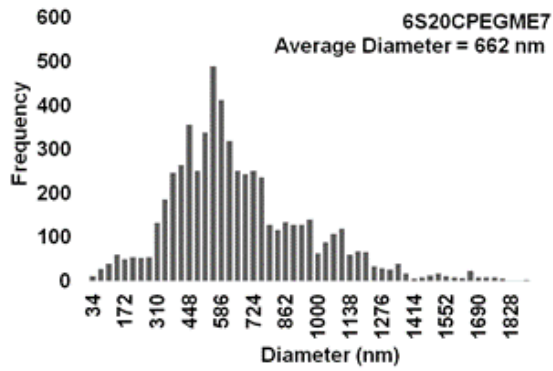
Mostly the samples which were produced using 6wt% PAN as a shell displayed smoother nanofibers. They were beadless and cylindrical in shape but increase in shell concentration generally resulted with the increase in average diameter of nanofibers. As a result, 14 nanowebs have an average diameter smaller than 1 μm and 10 nanowebs have an average diameter smaller than 500 nm, indicating successful production of nanofibers. Moreover, generally beadless, smooth and cylindrical nanofiber production is achieved with all variations of shell and core solution concentrations.

#### 4.2.2.2 SEM of PAN/PEGME nanowebs

The SEM images and diameter distribution analysis of PAN/PEGME nanowebs are given in Figure 4.7 and 4.8, through two samples.

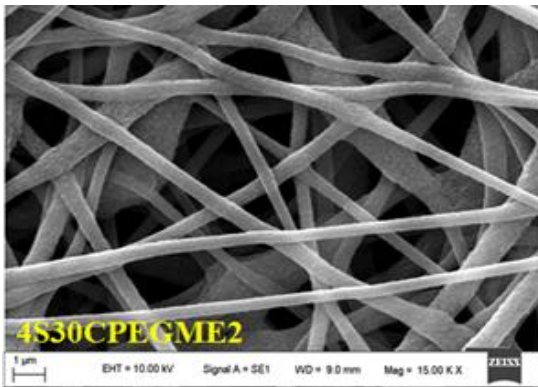


(a)

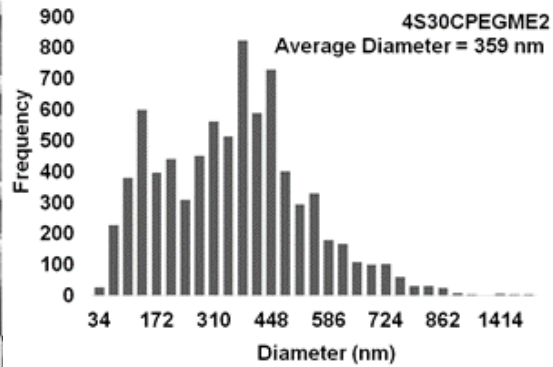


(b)

**Figure 4.7 :** (a) SEM image of 6S20CPEGME7 nanoweb. (b) Diameter distribution histogram of 6S20CPEGME7 nanoweb.



(a)



(b)

**Figure 4.8 :** (a) SEM image of 4S30CPEGME2 nanoweb (b) Diameter distribution histogram of 4S30CPEGME2 nanoweb.

SEM images of PAN/PEGME nanoweb showed generally beadless, smooth and cylindrical nanofibers. In accordance with nanofiber diameter distributions: average diameter value of 4S20CPEGME3 (B3) nanoweb centered around 280-300 nm; average diameter value of 4S30CPEGME1 (B1), 4S30CPEGME2 (B2) and 4S20CPEGME4 (B4) nanoweb centered around 301-500 nm, and rest of them centered in a range from 501-939 nm.

Nanoweb which were produced using 6wt% PAN as a shell displayed higher average diameter values. As a result, 4 nanoweb have an average diameter smaller than 1 μm and 4 nanoweb have an average diameter smaller than 500 nm indicating successful production of nanofibers. Moreover, generally beadless, smooth and cylindrical nanofiber production was achieved with all variations of shell and core solution concentrations.



#### 4.2.2.3 SEM of PAN/*n*-alkane nanowebs

Figure 4.9 and 4.10 shows, SEM images and diameter distribution analysis for two nanowebs composed of PAN/*n*-alkane.

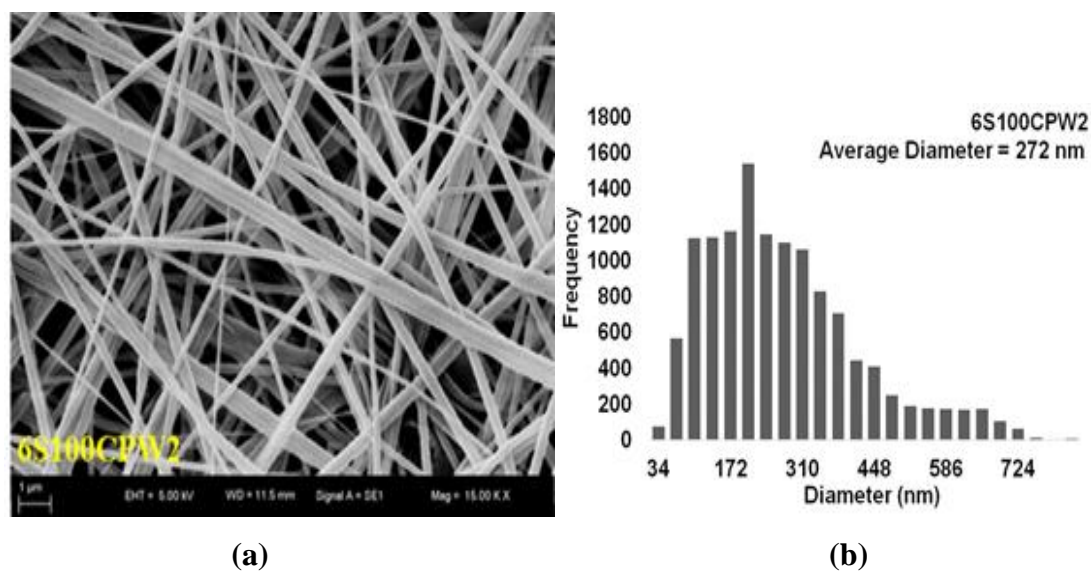


**Figure 4.9 :** (a) SEM image of 6S100CPW2 nanoweb. (b) Diameter distribution histogram of 6S100CPW2 nanoweb.

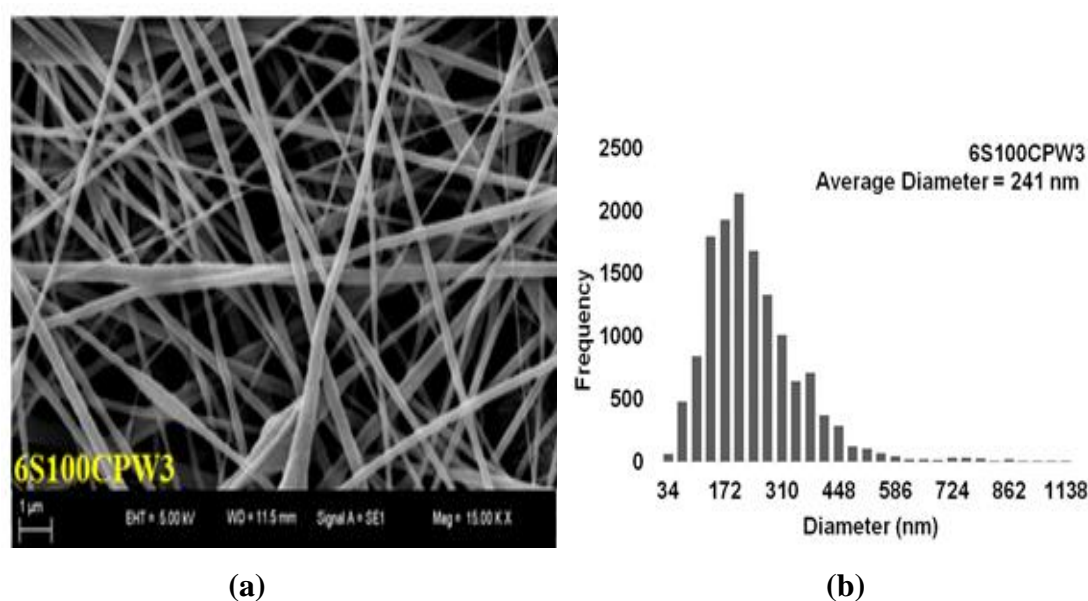


**Figure 4.10 :** (a) SEM image of 6S100CPW3 nanoweb. (b) Diameter distribution histogram of 6S100CPW3 nanoweb.

SEM images of PAN/*n*-alkane nanowebs demonstrated generally beadless, smooth and cylindrical nanofibers. According to diameter analysis, all PAN/*n*-alkane nanowebs showed similar average diameter values smaller than 300 nm.

#### 4.2.2.4 SEM of nanoweb produced from synthesized copolymers

In this part, the results of nanoweb produced from the mixtures of synthesized PEG-MAH-g-PAN grafted copolymer and PAN solution and made of hollow nanofibers are given.

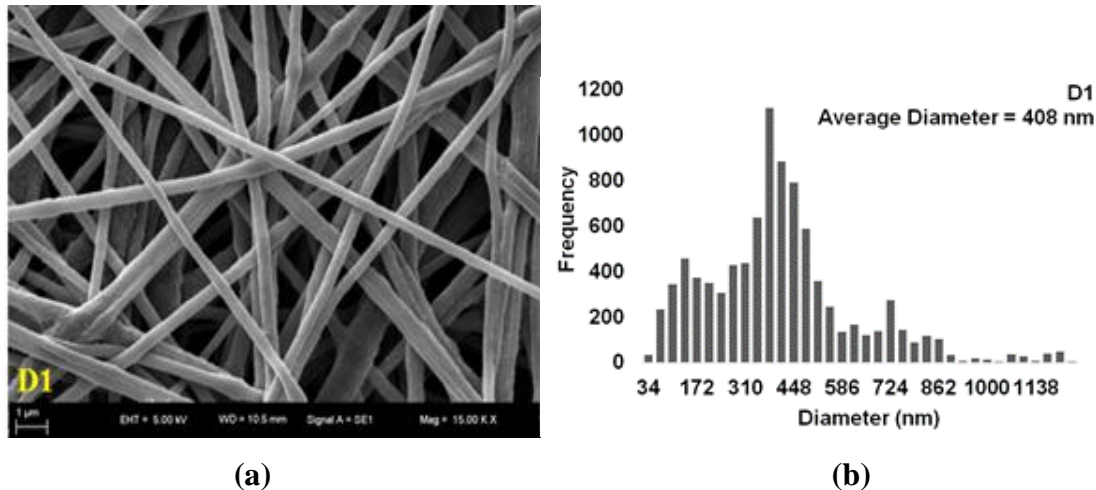


**Figure 4.11 :** (a) SEM image of D1 nanoweb. (b) Diameter distribution histogram of D1 nanoweb.

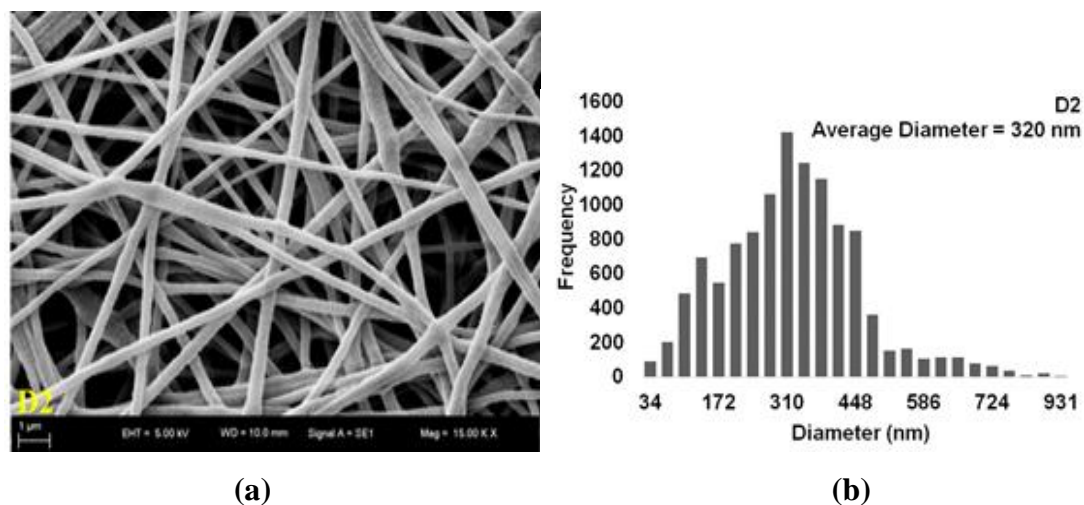


**Figure 4.12 :** (a) SEM image of D2 nanoweb. (b) Diameter distribution histogram of D2 nanoweb.

Figure 4.11 and 4.12 give the SEM images and diameter distribution analysis for two nanoweb composed of PEG-MAH-g-PAN copolymer. The SEM images and diameter distribution analysis showed that beadless, smooth and cylindrical nanofiber production was achieved with the average diameters of 408 nm and 320 nm for D1 and D2 nanoweb, respectively.

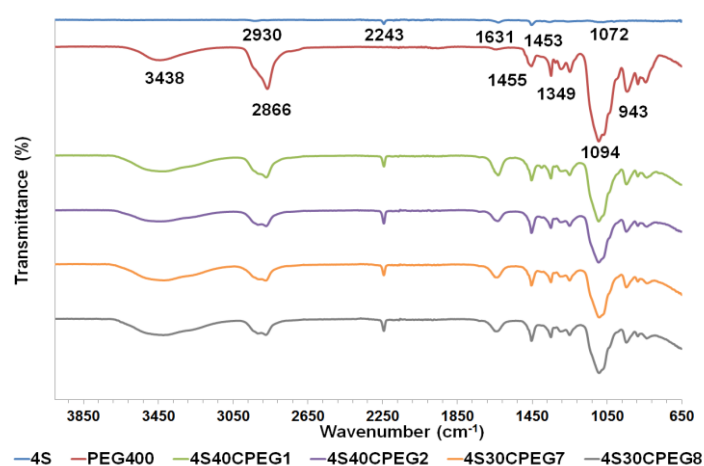


### 4.2.3 Fourier transform infrared spectroscopy (FTIR) results

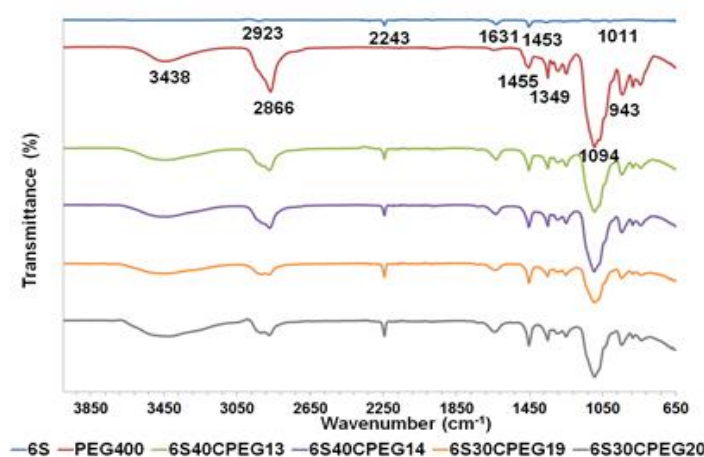
FTIR analysis were performed for shell, core materials and for produced nanoweb. FTIR graphs are arranged comparatively based on control groups, pure core material and produced bicomponent nanoweb using these materials.

#### 4.2.3.1 FTIR of PAN/PEG nanoweb

Figure 4.13a and b shows FTIR graph of 4S control group, PEG400, produced nanoweb from 4S/PEG400 combination and 6S control group, PEG400, produced nanoweb from 6S/PEG400 combination, respectively.



(a)



(b)

**Figure 4.13 :** The comparative FTIR spectra of: (a) 4S, PEG400 and 4S/PEG400 nanoweb. (b) 6S, PEG400 and 6S/PEG400 nanoweb.

The produced nanoweb from 4wt% PAN and 6wt% PAN solutions were used as the control groups and they named as 4S and 6S, respectively. Both 4S and 6S also

demonstrated typical bands of PAN on FTIR spectra. The FTIR spectra of control groups showed characteristic transmission bands for stretching and bending vibrations of CH<sub>2</sub> groups at 2915–2882 cm<sup>-1</sup> and 1455 cm<sup>-1</sup>, respectively. Likewise pure PAN. The stretching vibration of nitrile (C≡N) groups in PAN chains give a strong transmission band at 2243 cm<sup>-1</sup>, while 1072 cm<sup>-1</sup> band was associated with the bending vibration of C–N groups. All of these vibrations appeared as distinct bands in the FTIR spectra of 4S/PEG400 and 6S/PEG400 nanoweb, indicating the presence of PAN in the nanoweb composition. Likewise, the band at 2866 cm<sup>-1</sup> that correspond to the stretching vibrations of the –CH<sub>2</sub> groups of the PEG chains appeared in the spectra of the nanoweb (Fig. 4a and 4b). The –CH<sub>2</sub> bending vibration band at 1455 cm<sup>-1</sup> and the –CH rocking band at 1349 cm<sup>-1</sup> of the PEG chains overlapping with those of PAN appeared as distinct bands in the FTIR spectra of the 4S/PEG400 and 6S/PEG400 nanoweb. The bands at 1279 cm<sup>-1</sup>, 1094 cm<sup>-1</sup>, 943 cm<sup>-1</sup> corresponding to the C–O–C stretching vibrations of ether groups in the PEG chains are also existed in the FTIR spectrum of the 4S/PEG400 and 6S/PEG400 nanoweb.

FTIR spectra of 4S/PEG600, 6S/PEG600, 4S/PEG1000 and 6S/PEG1000 nanoweb showed also all typical transmission bands of their corresponding shell and core materials. Figure 4.14 shows the FTIR spectra of 6S control group, PEG1500, produced nanoweb from 6S/PEG61500 combination.

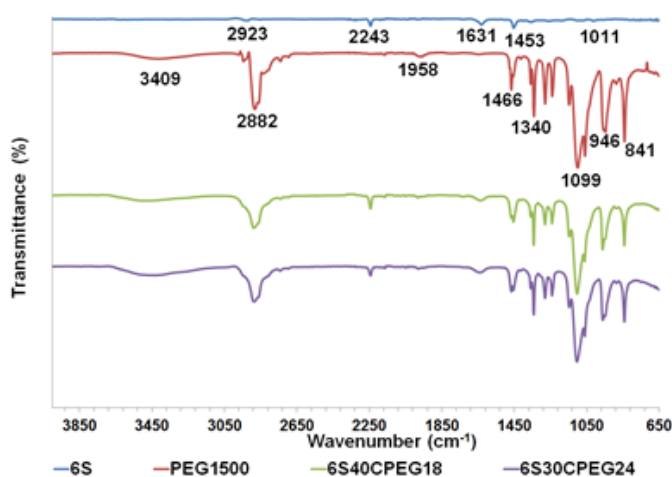


**Figure 4.14 :** The comparative FTIR spectra 6S, PEG1500 and 6S/PEG1500 nanoweb.

FTIR spectra of 6S/PEG1500 nanoweb and 4S/PEG1500 nanoweb showed also all typical transmission bands of their corresponding shell and core materials which are PAN and PEG1500.

Consequently, all characteristic bands of PAN and PEG appeared in the FTIR spectra of electrospun PAN-PEG nanoweb, with no new peak being formed, approving that PAN and PEG did not interact anyway, and PEG cores were successfully encapsulated in PAN shells to give PAN-PEG nanoweb, preventing leakage of PEG from the PAN matrix.

#### 4.2.3.2 FTIR of PAN/PEGME nanoweb

FTIR spectra of nanoweb produced from PAN/PEGME combination are given in comparison with their corresponding control groups and core materials. Figure 4.15a and 4.15b illustrate FTIR spectra of 4S control group, PEGME550, produced nanoweb from 4S/PEGME550 combination and 4S control group, PEGME750, nanoweb produced from 4S/PEGME750 combination, respectively.

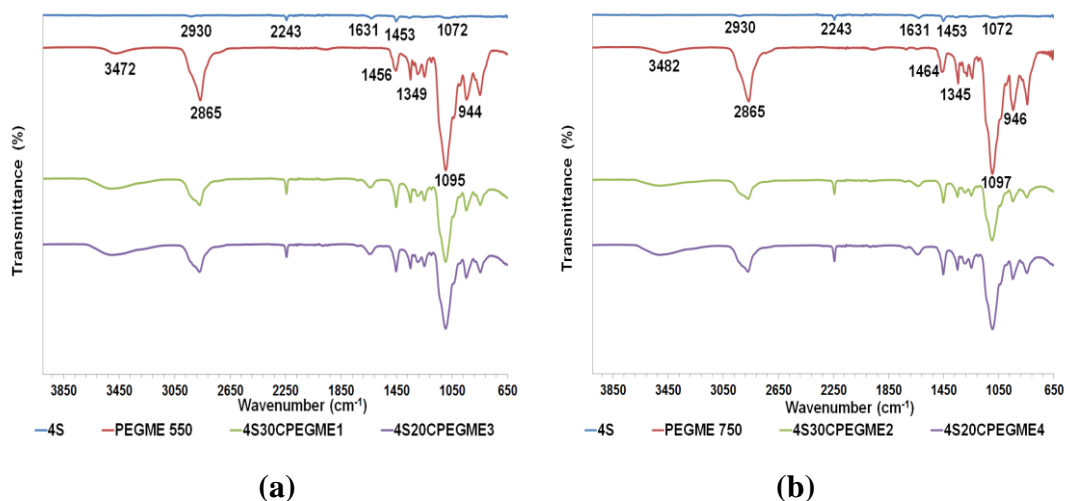


**Figure 4.15 :** The comparative FTIR spectra of: (a) 4S, PEGME550 and 4S/PEGME550 nanoweb. (b) 4S, PEGME750 and 4S/PEGME750 nanoweb.

It can be seen from comparative graphs that all nanoweb composed of PAN/PEGME were displayed the typical PAN bands at 2923-2930  $\text{cm}^{-1}$ , 2243  $\text{cm}^{-1}$ , 1631  $\text{cm}^{-1}$ , 1453  $\text{cm}^{-1}$  and 1072-1011  $\text{cm}^{-1}$ . The FTIR spectra of PEGME chains also showed similar bands with PEG chains because of the molecular similarity. The band at 2865  $\text{cm}^{-1}$  that corresponds to the stretching vibrations of the  $-\text{CH}_2$  groups of the PEGME chains. The typical bands at 1456  $\text{cm}^{-1}$  and at 1349  $\text{cm}^{-1}$  refers to  $-\text{CH}_2$  bending vibration and the  $-\text{CH}$  rocking band, respectively. The bands at 1095  $\text{cm}^{-1}$ , 944  $\text{cm}^{-1}$  corresponding to the C-O-C stretching vibrations of ether groups in the PEGME chains.

Considering comparative FTIR spectra, all typical bands of both PAN and PEGME was appeared as overlapping or distinct bands in the FTIR spectra of the corresponding PAN/PEGME nanoweb.

#### 4.2.3.3 FTIR of PAN/*n*-alkane nanoweb

Figure 4.16 shows FTIR spectra of 6S control group, *n*-alkanes, say *n*-pentadecane and *n*-hexadecane with produced nanoweb corresponding 6S/*n*-alkane combination.

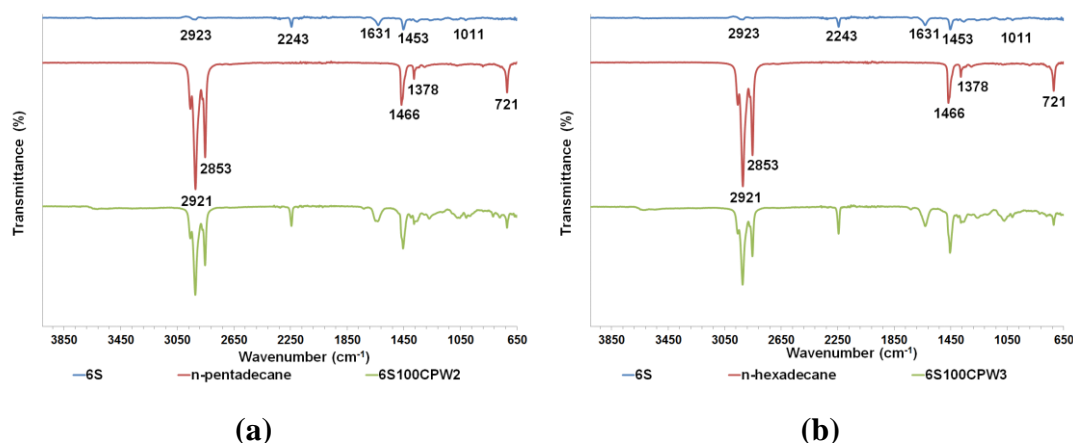
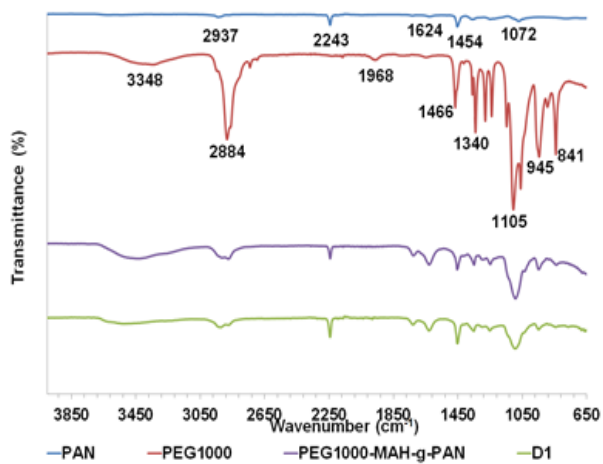


**Figure 4.16 :** The comparative FTIR spectra of: (a) 6S, *n*-pentadecane and 6S100CPW2 nanoweb. (b) 6S, *n*-hexadecane and 6S100CPW3 nanoweb.

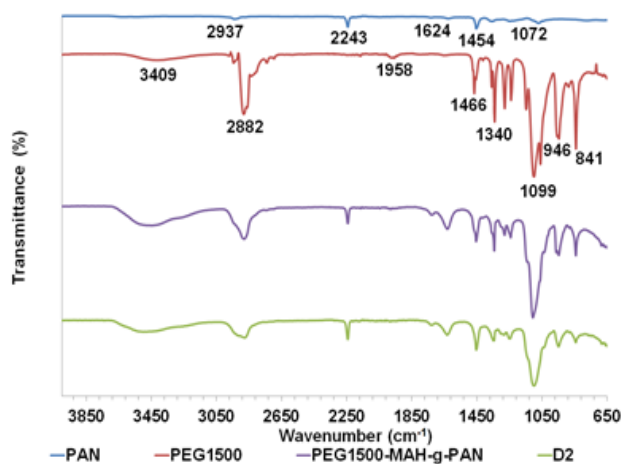
The simple *n*-alkanes have very few bands in FTIR spectra and they are generally characterized by absorptions due to C–H stretching and bending. All *n*-alkanes used as a core material have multiple transmission bands around 2955, 2921 and 2853  $\text{cm}^{-1}$  associated with asymmetric and symmetric stretching vibrations of  $\text{CH}_2$  groups of alkane chains. The bands around 1466  $\text{cm}^{-1}$  and 1379  $\text{cm}^{-1}$ , which were also displayed by all alkanes, refer to bending vibrations and rocking vibrations of  $-\text{CH}_3$  groups, respectively. In long chain alkanes there is also rocking vibrations of  $-\text{CH}_3$  at bands around 721  $\text{cm}^{-1}$  which can be seen again in spectrum of used *n*-alkanes. All of these vibrations appeared as distinct bands in the FTIR spectra of PAN/*n*-alkane nanoweb, indicating the presence of corresponding *n*-alkane in the nanoweb composition. Besides, the typical PAN bands at 2923-2930  $\text{cm}^{-1}$ , 2243  $\text{cm}^{-1}$ , 1631  $\text{cm}^{-1}$ , 1453  $\text{cm}^{-1}$  and 1072-1011  $\text{cm}^{-1}$  were also displayed by PAN/*n*-alkane nanoweb approving that presence of PAN in the nanoweb composition, too.

#### 4.2.3.4 FTIR of synthesized copolymers and nanoweb produced from them

Figure 4.17 indicates the comparative FTIR spectra of these synthesized grafted copolymers, PAN, their corresponding PEG and nanoweb.



(a)



(b)

**Figure 4.17 :** FTIR spectra of: (a) D1 nanoweb in comparison with PEG1000-MAH-g-PAN, pure PAN and PEG1000. (b) D2 nanoweb in comparison with PEG1500-MAH-g-PAN, pure PAN and PEG1500.

Comparative FTIR spectra showed that typical bands of both PAN and PEG are appeared in the FTIR spectra of synthesized copolymer clearly. At the same time, the typical bands of PAN and PEG-MAH-g-PAN existed in the FTIR spectra of produced nanoweb. In FTIR spectra of both nanoweb, there is an increase in the intensity of band at 2243 cm<sup>-1</sup> due to the increasement in the amount of PAN with using mixture of PAN and PEG-MAH-g-PAN solutions.

### 4.3 Thermal Characterization Results

#### 4.3.1 Differential scanning calorimetry (DSC) results of core materials

The DSC analysis results of PCMs used as a core material are shown in Table 4.2. DSC analysis were performed for 10 heating-cooling cycle for each PCM, at the rate of 10 °C.min<sup>-1</sup>.

**Table 4.2 :** DSC results of PCMs for 2<sup>nd</sup> and 10<sup>th</sup> cycles.

PCM	2 <sup>nd</sup> Heating				2 <sup>nd</sup> Cooling				10 <sup>th</sup> Heating				10 <sup>th</sup> Cooling			
	Phase transition temperatures (°C)			$\Delta H$ (Jg <sup>-1</sup> )	Phase transition temperatures (°C)			$\Delta H$ (Jg <sup>-1</sup> )	Phase transition temperatures (°C)			$\Delta H$ (Jg <sup>-1</sup> )	Phase transition temperatures (°C)			$\Delta H$ (Jg <sup>-1</sup> )
	T <sub>onset</sub>	T <sub>peak</sub>	T <sub>end</sub>		T <sub>onset</sub>	T <sub>peak</sub>	T <sub>end</sub>		T <sub>onset</sub>	T <sub>peak</sub>	T <sub>end</sub>		T <sub>onset</sub>	T <sub>peak</sub>	T <sub>end</sub>	
PEG400	-11	5	8	83	-11	-13	-18	87	-10	5	8	88	-11	-13	-17	90
PEG600	8	19	23	135	12	7 4	-3	135	11	22	25	139	12	9 4	1	138
PEG1000	30	38	41	160	26	22	14	159	31	39	41	165	28	22	14	161
PEG1500	37	46	51	163	26	22 17	12	161	40	47	52	165	25	20	15	161
PEGME550	-7	14	19	136	9	4	-12	136	-1	18	21	160	10	6	-22	146
PEGME750	7	23	31	73	23	20 15	2	73	7	27	32	80	23	18	4	77
<i>n</i> -tetradecane (C <sub>14</sub> H <sub>30</sub> )	5	11	13	246	-2	-5	-8	244	4	10	12	247	-1	-5	-8	245
<i>n</i> -pentadecane (C <sub>15</sub> H <sub>32</sub> )	-3	-1	1	45	5	0	-3	182	-4	-1	0	45	5	0	-3	183
<i>n</i> -hexadecane (C <sub>16</sub> H <sub>34</sub> )	17	22	25	237	15	11	8	240	17	22	25	237	15	11	8	239
<i>n</i> -heptadecane (C <sub>17</sub> H <sub>36</sub> )	12	14	17	43	21	15	11	175	11	14	17	43	21	15	11	173
<i>n</i> -octadecane (C <sub>18</sub> H <sub>38</sub> )	22	28	32	162	9	6	4	40	22	28	32	161	9	6	4	39
<i>n</i> -octadecane (C <sub>18</sub> H <sub>38</sub> )	30	34	37	255	24	20	18	254	30	34	37	254	23	20	17	253

Each PCM demonstrated a phase transition from solid to liquid state and from liquid to solid state, which were taking place at almost the same temperature intervals during 10 subsequent heating and cooling process. Heating curves and cooling curves overlapped within themselves from 2<sup>nd</sup> to 10<sup>th</sup> cycle, indicating thermal stability of each of the PCM. While cooling, phase change shifted to a lower interval during solidification process, reminding the difficulty of crystallization of the PCM chains. Enthalpies also remained almost same in the 10th heating-cooling cycle. Thus, phase transition characteristics and the high heat storage capacities of each PCM were found suitable for nanoweb applications. Moreover, DSC results of PEG400, PEGME550,

*n*-tetradecane and *n*-pentadecane were suitable for the use in cold region applications and others are suitable for the normal region applications.

### 4.3.2 Differential scanning calorimetry (DSC) results of nanowebs

#### 4.3.2.1 DSC of PAN nanowebs

Two different nanowebs were produced using 4wt% PAN solution and 6wt% PAN solution in DMAc to use them as a control group named 4S and 6S, respectively. Figure 4.21 shows comparative DSC results for 2<sup>nd</sup> heating-cooling cycle of PAN copolymer, 4S and 6S control group.

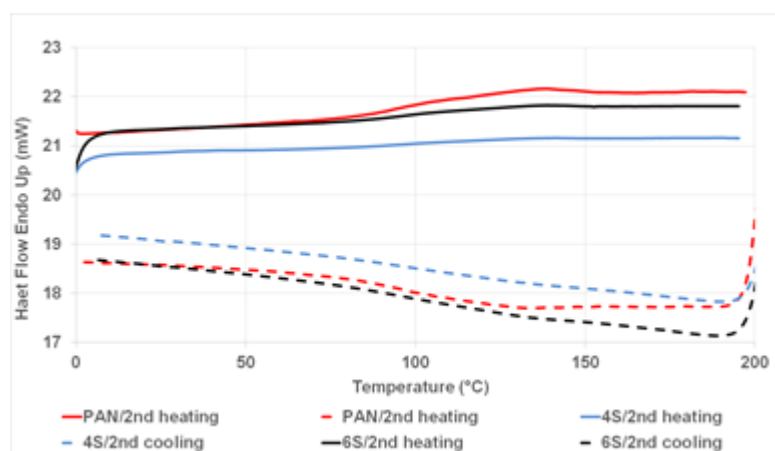


**Figure 4.18 :** The comparative DSC graphs of PAN, 4S and 6S for 2<sup>nd</sup> cycle; at the rate of 10°C.min<sup>-1</sup>.

DSC graphs showed that neither 4S nor 6S nanowebs displayed a phase transition or an enthalpy change during heating and cooling processes likewise pure PAN copolymer. This thermal analysis was taken into consideration as a reference to characterize the nanowebs produced from PAN shell.

#### 4.3.2.2 DSC of PAN/PEG nanowebs

In electrospinning experiments of PAN/PEG400 and PAN/PEG600, 1wt% of PEG1000 or PEG1500 was added alternately to 30wt% and 40wt% PEG400 and PEG600 solutions with the aim of making more thermally stable nanowebs. The nanowebs containing PEG400 or PEG600 performed phase transitions repeatedly in cyclic DSC analyses while keeping their thermal stability and achieving considerable heat capacities during in both heating and cooling processes.

Figure 4.19a and b represents DSC graphs of PAN/PEG400 nanoweb in comparison with pure PEG400, for 4<sup>th</sup> heating and cooling cycle.

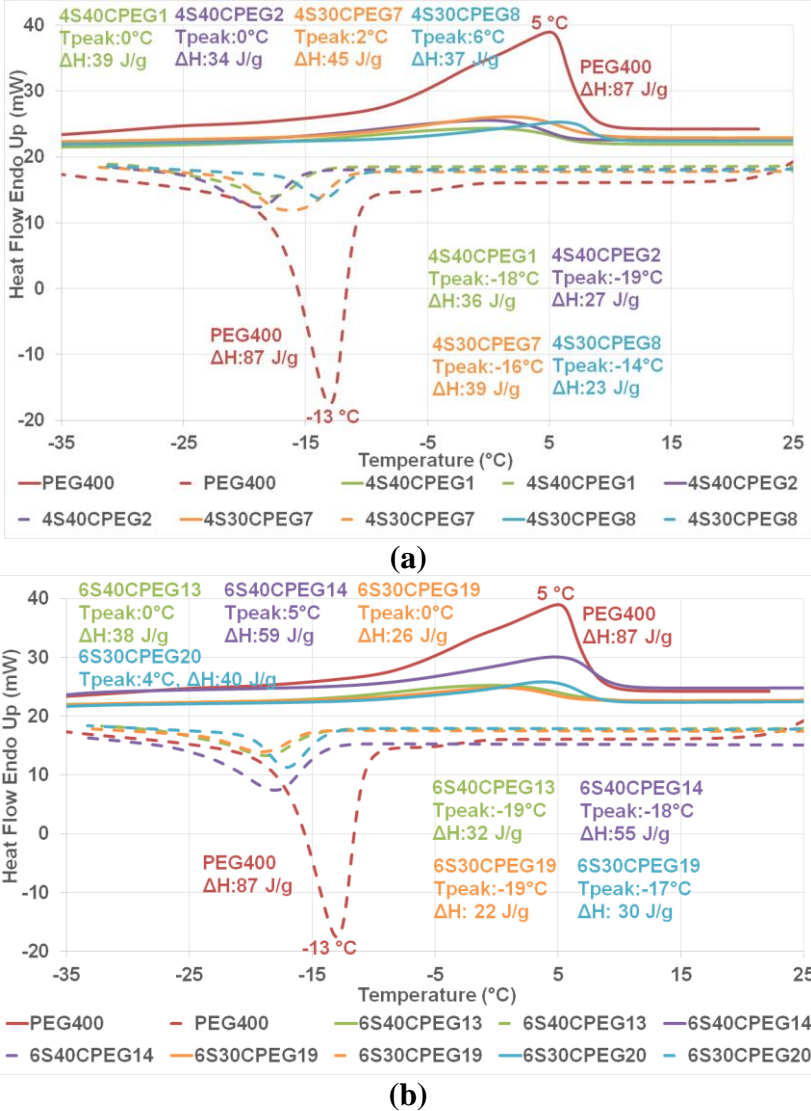
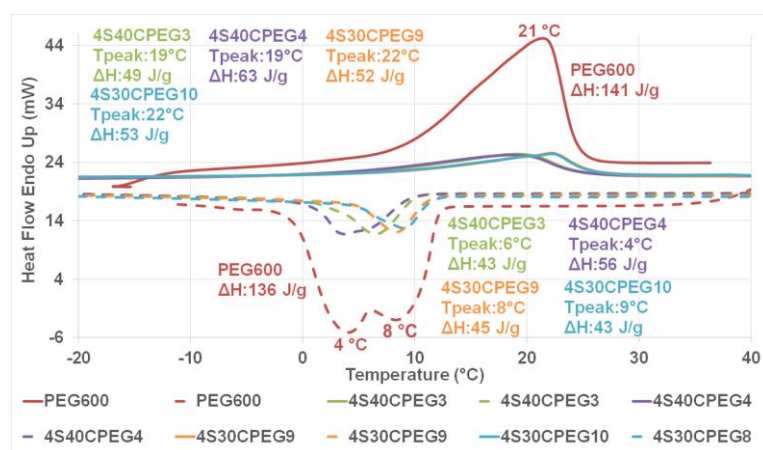


**Figure 4.19 :** The DSC graphs of PAN/PEG400 nanoweb in comparison with pure PEG400: (a) 4PAN/PEG400 nanoweb. (b) 6PAN/PEG400 nanoweb.

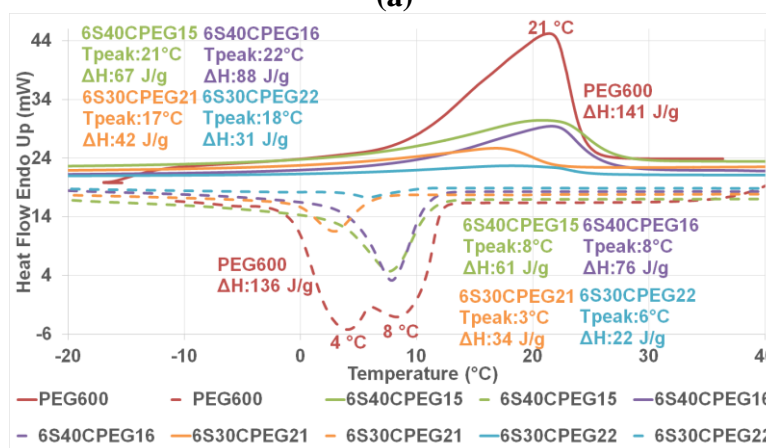
DSC graphs in Figure 4.19a and b showed that all PAN/PEG400 nanoweb displayed considerable heat capacities in both heating and cooling processes greatly overlapping phase transition interval of pure PEG400 thanks to the successful encapsulation of PEG400 by PAN shells. When DSC results of PAN/PEG400 nanoweb were compared with that of pure PEG400, phase transition intervals of nano structured composites slightly shifted toward 1-2 °C higher temperatures during heating probably because using (wt%) either 40:1 or (wt%) 30:1 mixture of PEG400 and PEG1000 or PEG1500. While cooling, phase transitions of nanoweb shifted to slightly lower



temperatures reminding supercooling taking place due to the composite structures of them. Considering DSC results, PAN/PEG400 nanowebbs have phase transition interval that began from -23°C and ended at 8-10°C, with peak temperatures between -4 – 6°C. The 6S40CPEG14 (A14) nanoweb performed best result with having latent heat of fusion of 59 J.g<sup>-1</sup>. Figure 4.20a and b shows DSC graphs of PAN/PEG600 nanowebbs in comparison with pure PEG600, for 4<sup>th</sup> heating and cooling cycle.



(a)



(b)

**Figure 4.20 :** The DSC graphs of PAN/PEG600 nanowebbs in comparison with pure PEG600: (a) 4PAN/PEG600 nanowebbs. (b) 6PAN/PEG600 nanowebbs.

From DSC results of nanowebbs given in Figure 4.20 it can be seen that, PAN/PEG600 nanowebbs have heat capacities of a minimum 29 Jg<sup>-1</sup> and a maximum 88 Jg<sup>-1</sup> during heating process and of a minimum 22 Jg<sup>-1</sup> and a maximum 74 Jg<sup>-1</sup> heat capacities during cooling processes. In this experiment also there was formation of new PEG mixture in every successive heating-cooling process with contribution of added 1wt% PEG1000 and PEG1500. Therefore, in 4<sup>th</sup> heating processes melting began from slightly higher temperature value for all nanowebbs. The 6S40CPEG16 (A16) nanoweb

has shown best heat capacity result which is  $88 \text{ Jg}^{-1}$ . Comparative DSC graphs indicated that all PAN/PEG600 nanowebs have shown heat capacity both in heating and cooling processes with similar phase transition interval as pure PEG600 indicating successful encapsulation of PEG600 by PAN shells. The comparative DSC graphs of PAN/PEG1000 nanowebs in comparison with pure PEG1000, for 4<sup>th</sup> heating and cooling cycle are given in Figure 4.21a and b.

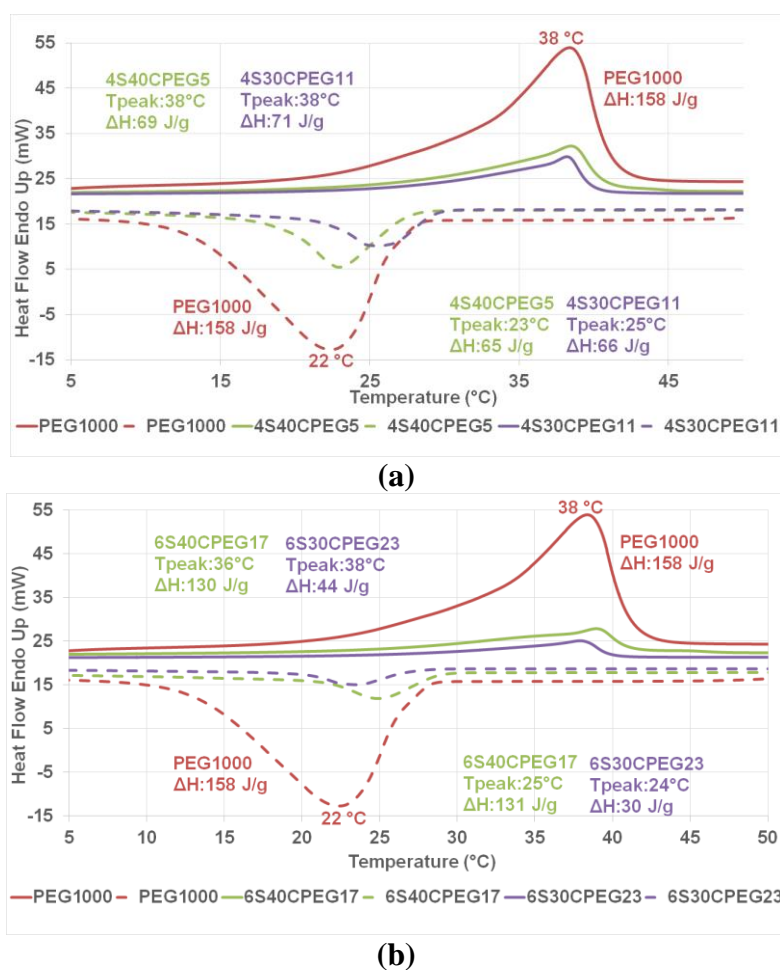
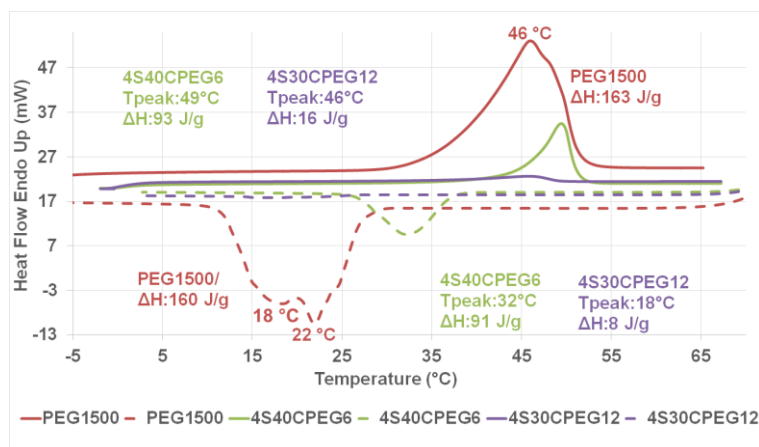


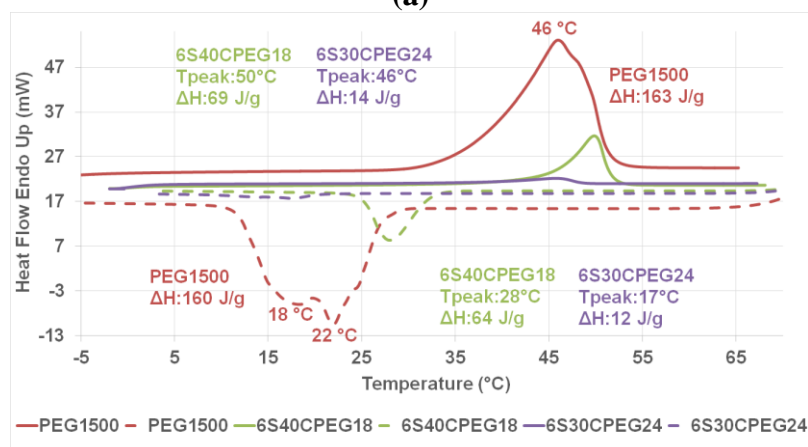
**Figure 4.21 :** The DSC graphs of PAN/PEG1000 nanowebs in comparison with pure PEG1000: (a) 4PAN/PEG1000 nanowebs. (b) 6PAN/PEG1000 nanowebs.

DSC graphs of PAN/PEG1000 nanowebs in comparison pure PEG1000 showed that phase transition intervals and heat capacities for heating and cooling processes are preserved indicating achievement of encapsulation by electrospinning (Figure 4.21). The nanowebs composed of PAN shell and PEG1000 core have demonstrated heat capacities varied between 28-131  $\text{Jg}^{-1}$  in successive 4 heating-cooling cycles. Because of shell/core composite structure there are some slightly shifted melting and solidification temperatures for all nanowebs compare to those of pure PEG1000. The

6S40CPEG17 (A17) nanoweb has shown the highest latent heat of fusion value with  $131 \text{ Jg}^{-1}$ . Figure 4.22a and b indicate DSC graphs of PAN/PEG1500 nanoweb in comparison with pure PEG1500, for 4<sup>th</sup> heating and cooling cycle.



(a)



(b)

**Figure 4.22 :** The DSC graphs of PAN/PEG1500 nanoweb in comparison with pure PEG1500: (a) 4PAN/PEG1500 nanoweb. (b) 6PAN/PEG1500 nanoweb.

All PAN/PEG1500 nanoweb given in Figure 4.22 showed heat capacities with a minimum  $13 \text{ Jg}^{-1}$  and a maximum  $93 \text{ Jg}^{-1}$ . There was also some small variations in phase transition intervals of nanoweb from pure PEG1500 because of composite structure of nanoweb. However, these nanoweb have shown better thermal stability during 4 successive heating-cooling cycle with almost same phase transition intervals and heat capacities. The highest latent heat of fusion value of  $93 \text{ Jg}^{-1}$  was obtained with 4S40CPEG6 (A6) nanoweb. Comparative DSC graphs for PAN/PEG1500 nanoweb with pure PEG1500 demonstrated similar achievement with other PAN/PEG applications.

As a result of DSC analysis of all bicomponent PAN/PEG shell/core nanoweb structure there were achieved minimum  $9 \text{ Jg}^{-1}$  and maximum  $77 \text{ Jg}^{-1}$  heat capacities with PEG400 and PEG600 which can be used in cold region applications. As well as there were achieved minimum  $13 \text{ Jg}^{-1}$  and maximum  $131 \text{ Jg}^{-1}$  heat capacities with PEG1000 and PEG1500 which can be used in normal region applications.

**4.3.2.3 DSC of PAN/PEGME nanoweb**

Figure 4.23a and b shows DSC graphs of PAN/PEGME550 nanoweb in comparison with pure PEGME550, for 4<sup>th</sup> heating and cooling cycle.

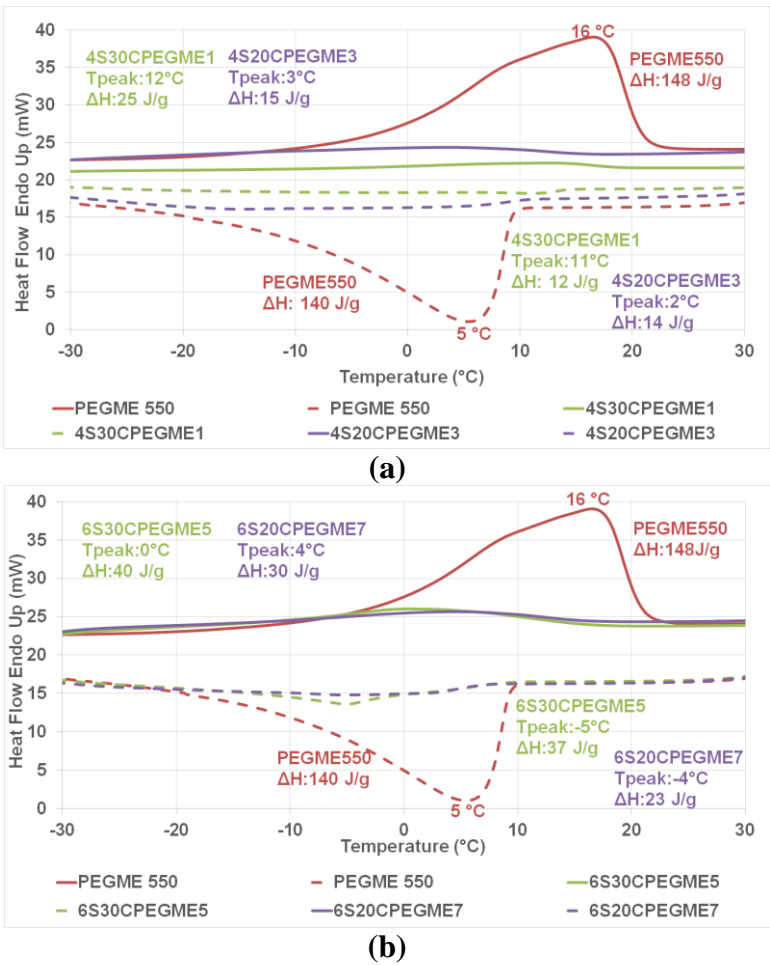
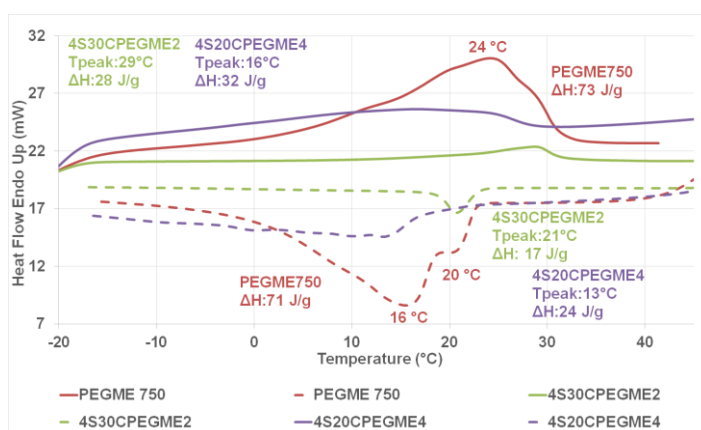


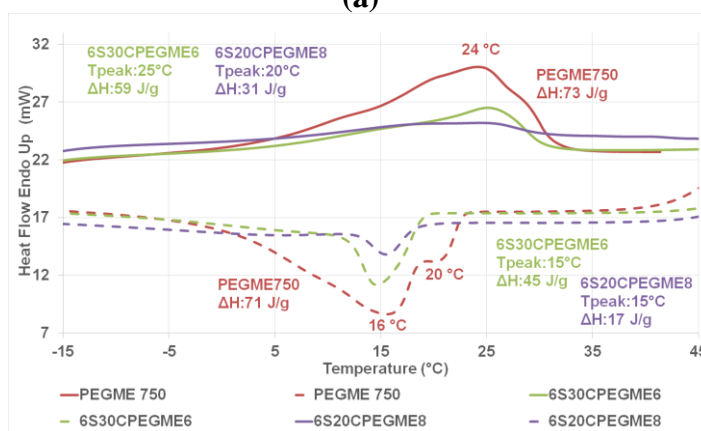
**Figure 4.23 :** The DSC graphs of PAN/PEGME550 nanoweb in comparison with pure PEGME550: (a) 4PAN/PEGME550 nanoweb. (b)6PAN/PEGME550 nanoweb.

According to the results, phase transition intervals and T<sub>peak</sub>'s were shifted to the lower temperatures in nanoweb according to pure PEGME550 due to the composite structure of nanoweb. Considering all PAN/PEGME550 nanoweb, the phase transition in heating processes began from -17 °C as a minimum and ended at 19 °C as

a maximum with  $T_{\text{peak}}$ 's of varying between  $-1 - 12\text{ }^{\circ}\text{C}$ . The nanoweb demonstrated heat capacities of minimum  $7\text{ Jg}^{-1}$  and maximum  $40\text{ Jg}^{-1}$ . The 6S30CPEGME5 (B5) nanoweb has the highest latent heat of fusion. Comparative DSC graphs showed that all PAN/PEGME550 nanoweb performed enthalpies in both heating and cooling processes with similar phase transition interval as pure PEGME550 indicating successful encapsulation of PEGME550 by PAN shells. The comparative DSC graphs of PAN/PEGME750 nanoweb in comparison with pure PEGME750, for 4<sup>th</sup> heating and cooling cycle are given in Figure 4.24a and b.



(a)



(b)

**Figure 4.24 :** The DSC graphs of PAN/PEGME750 nanoweb in comparison with pure PEGME750: (a) 4PAN/PEGME750 nanoweb. (b) 6PAN/PEGME750 nanoweb.

Overlapped DSC graphs of all PAN/PEGME750 nanoweb displayed heat capacities in both heating and cooling processes with similar phase transition interval as pure PEGME750. DSC results of PAN/PEGME750 nanoweb indicated heat capacities varied between  $13 - 59\text{ Jg}^{-1}$  during 4 heating-cooling cycles. There were also some shifts on phase transition intervals of nanoweb according to pure PEGME750. The  $T_{\text{peak}}$  values of nanoweb were in between  $5 - 26\text{ }^{\circ}\text{C}$  for 2<sup>nd</sup> heating process and in

between 16 – 29 °C for 4<sup>th</sup> heating process. The 6S30CPEGME6 (B6) nanoweb has shown the highest heat capacity which is 59 Jg<sup>-1</sup>.

In according to PAN/PEGME nanoweb DSC results, there are achieved heat capacities and phase transition intervals suitable for both cold and normal region applications.

**4.3.2.4 DSC of PAN/*n*-alkane nanoweb**

Comparative DSC graphs of PAN/*n*-alkane nanoweb with corresponding pure *n*-alkane, at 4<sup>th</sup> heating and cooling cycle are given in Figure 4.25.

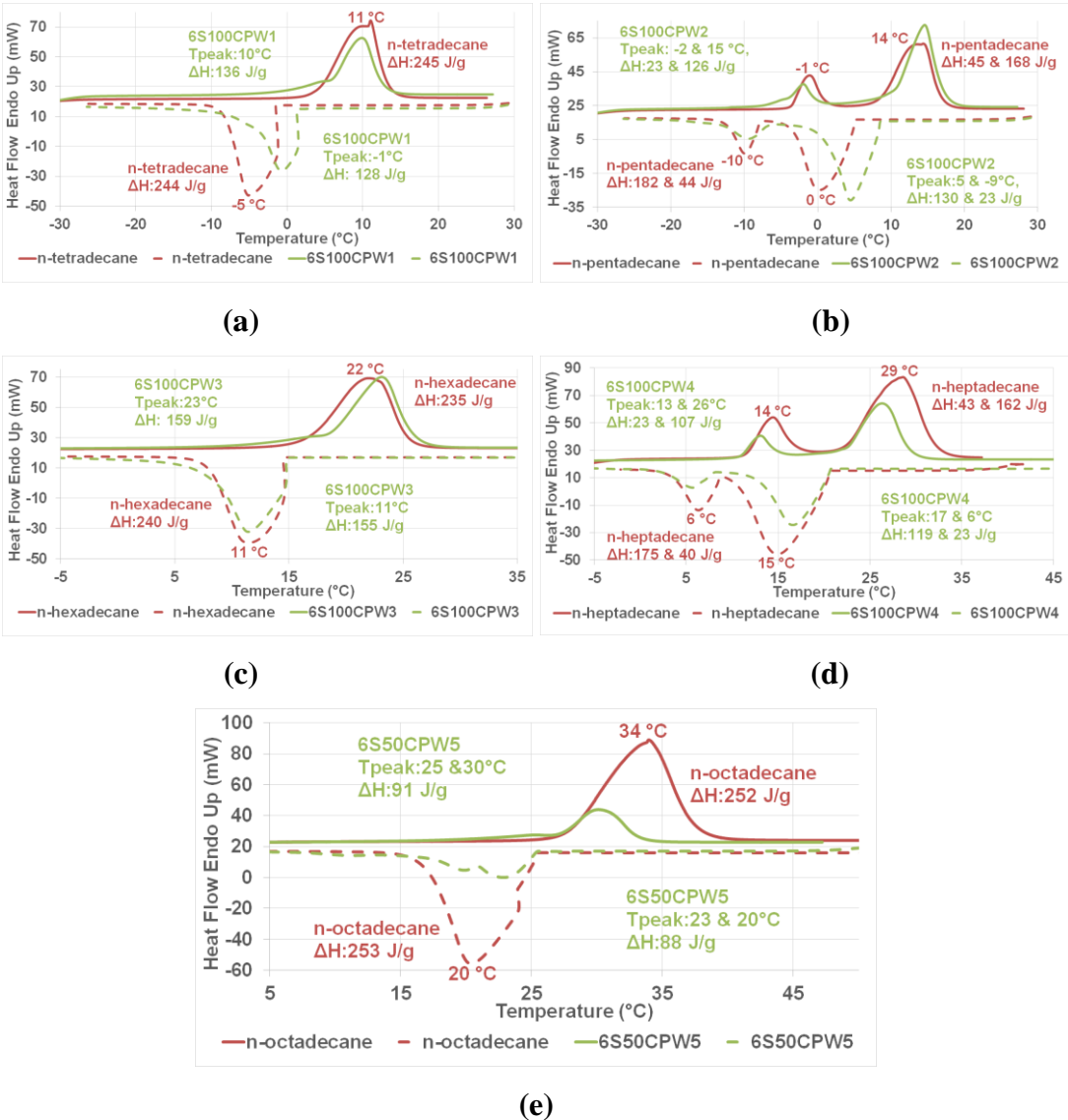


**Figure 4.25 :** The DSC graphs of PAN/*n*-alkane nanoweb in comparison with corresponding pure *n*-alkane.

All nanoweb have very sufficient latent heat of fusion with good thermal stability for both cold and normal region applications. There were almost same phase transition

ranges in composite nanoweb form according to pure *n*-alkanes and these intervals were kept same for all heating-cooling process in nanowebs. The heat capacities for heating-cooling processes were almost the same for all nanowebs and the achieved highest heat of fusion value is 159 Jg<sup>-1</sup> with 6S100CPW3 (C3) nanoweb. Comparative DSC graphs illustrate that all PAN/*n*-alkane nanowebs have very similar phase change behavior to that of corresponding pure *n*-alkane as an evidence of successful encapsulation of *n*-alkanes by PAN shells.

As a result of DSC analysis of PAN/*n*-alkane nanowebs, it can be seen that all of them demonstrated high heat capacities with minimum 91 Jg<sup>-1</sup> and maximum 159 Jg<sup>-1</sup> and thermal stability was achieved for both cold and normal region applications.

#### 4.3.2.5 DSC of nanowebs produced from synthesized grafted copolymers

The DSC results of 4<sup>th</sup> heating-cooling processes of nanowebs produced using synthesized grafted copolymers which are in the form of hollow nanofiber are given in Table 4.3. Both of the nanowebs kept their phase transition intervals and heat capacities almost the same up to 4<sup>th</sup> cycle, in both heating and cooling processes, which means that thermally stable nanowebs possessing solid-solid phase change feature were achieved. It can be seen that D1 nanoweb has heat capacity of 10 J.g<sup>-1</sup> between 24 – 39 °C with a T<sub>peak</sub> of 35-36 °C during heating, and has heat capacity of 6 J.g<sup>-1</sup> between 14 – -6 °C with a T<sub>peak</sub> of 5-6 °C during cooling. The D2 nanoweb has heat capacity of 19 J.g<sup>-1</sup> between 34 – 48 °C with a T<sub>peak</sub> of 46 °C during heating, and has heat capacity of 10 J.g<sup>-1</sup> between 23 – 9 °C with a T<sub>peak</sub> of 18 °C during cooling.

**Table 4.3 :** DSC analysis results of D1 and D2 nanowebs.

Nanoweb	4 <sup>th</sup> Heating				4 <sup>th</sup> Cooling			
	Phase transition temperatures (°C)			ΔH (Jg <sup>-1</sup> )	Phase transition temperatures (°C)			ΔH (Jg <sup>-1</sup> )
	T <sub>onset</sub>	T <sub>peak</sub>	T <sub>end</sub>		T <sub>onset</sub>	T <sub>peak</sub>	T <sub>end</sub>	
D1	24	36	39	10	13	5	-5	6
D2	35	46	48	19	23	18	11	10

Considering DSC results of all bicomponent shell/core nanoweb combinations were demonstrated considerable latent heat of fusions during successive heating processes and were showed latent heat of crystallizations during successive cooling process. Each nanoweb displayed similar phase transition interval as corresponding PCM material indicating the accomplished production of thermally stable nanowebs.





## 5. CONCLUSIONS AND RECOMMENDATIONS

In this study, various nanowebs composed of phase change material as a core and polyacrylonitrile as a shell were produced via coaxial electrospinning method. PAN/PCM nanocomposite nanowebs were manufactured using various shell/core concentrations. Moreover, solution of synthesized PEG-MAH-g-PAN grafted copolymer mixed with PAN solution and then used as a shell material to produce hollow nanofibers.

Electrospinning parameters were modified for each pair of shell/core combination after several trials and fine tunings. Thus, production of nanowebs for each pair was conducted with parameters where the Taylor Cone was obtained.

FTIR graphs of produced nanowebs demonstrated the typical peaks to be in accordance with those of corresponding core and shell materials as well as control sample for all cases. Results showed that there was not new peak being formed, approving that PAN and PCM did not interact anyway, and PCM cores were successfully encapsulated in PAN shells.

SEM images of nanowebs demonstrated that the accomplishment of beadless, smooth and cylindrical nanofibers are possible under the given electrospinning conditions for almost all samples with some exceptions where seldom bead formation was observed at 4% shell concentration. The diameter distribution analyses indicate that, average nano fiber diameter centered around 280-300 nm for ten samples; the diameter distributions of nine nanowebs centered around 301-500 nm, and rest of them centered in a range from 501 nm to 939 nm.

The DSC results of each nanoweb demonstrated considerable enthalpies in both heating and cooling processes, within similar temperature intervals of corresponding core material. Moreover, showing heat capacity feature during four successive heating and cooling processes indicated thermal stability of produced nanowebs. Table 5.1 indicates PAN/PCM nanoweb compositions and their corresponding application region depending on their melting temperature range during heating and cooling.

**Table 5.1 :** The nanoweb compositions and their corresponding application region.

Nanoweb Composition	Range of $T_{peak}$ (°C)		Corresponding Application Region
	During Heating	During Cooling	
PAN/PEG400	0 – 6	-20 – -14	Cold
PAN/PEG600	17 – 22	9 – 3	Normal
PAN/PEG1000	36 – 38	25 – 14	Normal
PAN/PEG1500	46 – 50	32 – 17	Normal
PAN/PEGME550	0 – 12	11 – -5	Cold
PAN/PEGME750	16 – 29	21 – 13	Normal
PAN/ <i>n</i> -tetradecane	10	-1	Cold
PAN/ <i>n</i> -pentadecane	-2	5	Cold
PAN/ <i>n</i> -hexadecane	15	-9	Cold
PAN/ <i>n</i> -heptadecane	23	11	Normal
PAN/ <i>n</i> -octadecane	13	17	Normal
	26	6	Normal
	25	23	Normal
	30	20	Normal

According to Table 5.1, the nanoweb containing core materials of PEG 400, PEGME550, *n*-tetradecane and *n*-pentadecane are suitable for cold region thermal applications and the nanoweb containing core materials of PEG600, PEG1000, PEG1500, PEGME750, *n*-hexadecane, *n*-heptadecane and *n*-octadecane are suitable for normal region thermal applications. The hollow nanofibers produced from PCM grafted PAN copolymers are promising as solid-solid nanoweb for normal region thermal applications.

The encapsulation ratios were evaluated from  $\Delta H_{nanoweb}/\Delta H_{PCM}$  ratio. The nanoweb having the highest enthalpy value among its PAN/PCM composition and their thermal properties are summarized in Table 5.2.

**Table 5.2 :** The encapsulation ratio of PCMs for nanoweb having highest enthalpy value among its PAN/PCM composition.

Nanoweb Sample	PCM	Melting Point (°C)	$\Delta H$ (J.g <sup>-1</sup> ) of		$\Delta H_{nanoweb}/\Delta H_{PCM}$ (%)
			PCM	Corresponding Nanoweb	
6S40CPEG14 (A14)	PEG400	5	88	59	68
6S40CPEG16 (A16)	PEG600	22	141	88	62
6S40CPEG17 (A17)	PEG1000	36	158	131	83
4S40CPEG6 (A6)	PEG1500	49	163	93	57
6S30CPEGME5 (B5)	PEGME550	0	148	40	27
6S30CPEGME6 (B6)	PEGME750	25	73	59	80
6S100CPW3 (C3)	<i>n</i> -hexadecane	23	235	159	63

Table 5.2 shows that the highest encapsulation ratio achieved by 6S40CPEG17 (A17) providing a melting enthalpy of 131 Jg<sup>-1</sup> at 36 °C which corresponds to 83% of the pure PEG1000.

The lowest encapsulation ratio achieved by 6S30CPEGME5 (B5), providing a melting enthalpy of  $40 \text{ Jg}^{-1}$  at  $0 \text{ }^\circ\text{C}$  which corresponds to 27% of the pure PEGME550.

In respect of this study, these nanowebs must be further studied by reinforcing them with some base textile surfaces or by using them as a layer of sandwich structures for the application fields such as cold packaging or thermally adaptive composite textiles for both cold and normal climates, regarding their structural characteristics and thermal performances.



## REFERENCES

- [1] **Onder, E., and Sarier, N.** (2012). Organic phase change materials and their textile applications: An overview. *Thermochimica Acta*, 540, 7-60.
- [2] **Mondal, S.** (2008). Phase change materials for smart textiles – An overview. *Applied Thermal Engineering*, 28, 1536-1550.
- [3] **Agarwal, S., Greiner, A. and Wendorff, J. H.** (2013). Functional materials by electrospinning of polymers. *Progress in Polymer Science*, 38, 963-991.
- [4] **Park, J. S.** (2010). Electrospinning and its applications. *Adv. Nat. Sci.: Nanosci. Nanotechnol.*, 1, 1-5.
- [5] **Onder, E., and Sarier, N.** (2015). Thermal regulation finishes for textiles. Woodhead Publishing Series in Textiles. *Functional Finishes for Textiles* (Vol. 2, pp. 18-76). Retrieved from <http://www.sciencedirect.com/science/article/pii/B9780857098399500029>
- [6] **Cabeza, L.F., Martorell, L. Miro, L., Fernandez, C. and Barreneche, C.** (2015). Introduction to thermal energy storage (TES) systems. Woodhead Publishing Series in Energy. *Advances in Thermal Energy Storage Systems* (Vol. 1, pp. 1-10). Retrieved from <http://www.sciencedirect.com/science/article/pii/B9781782420880500018>
- [7] **Pielichowska, K., and Pielichowski, K.** (2012). Phase change for thermal energy storage. *Progress in Polymer Science*, 65, 67-123.
- [8] **Mehling, H., and Cabeza, L. F.** (2008). Heat and cold storage with PCM. Springer-Verlag Berlin Heidelberg. *Heat and Mass Transfer*, pp. 1-52. Retrieved from <http://www.springer.com/us/book/9783540685562>
- [9] **Onder, E., and Sarier, N.** (2012). Organic phase change materials and their textile applications: An overview. *Thermochimica Acta*, 540, 7-60.
- [10] **Harris, J. M., Struck, E. C., Case, M. E. and Paley, M.S.** (1984). Synthesis and characterization of poly(ethylene glycol) derivatives. *Journal of Polymer Science: Polymer Chemistry Edition*, Vol. 22, 341-352.
- [11] **Gao, C.** (2014). Phase-change materials (PCMs) for warming or cooling in protective clothing. *Protective Clothing*, (Vol. 9, pp. 228-246). DOI: 10.1533/9781782420408.2.227

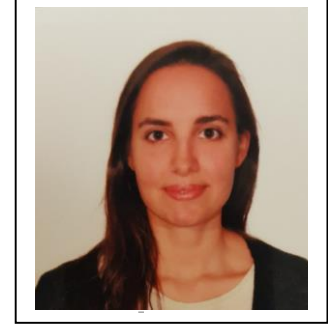
- [12] **Bruno, F., Belusko, M., Liu, M. and Tay, N. H. S.** (2015). Using solid-liquid phase change materials (PCMs) in thermal energy storage systems. Woodhead Publishing Series in Energy. *Advances in Thermal Energy Storage Systems* (Vol. 9, pp. 202-207). Retrieved from <http://www.sciencedirect.com/science/article/pii/B9781782420880500092>
- [13] **Bhardwaj, N. and Kundu, S. C.** (2010). Electrospinning: A fascinating fiber fabrication technique. *Biotechnology Advances*, 28, 325-347.
- [14] **Greiner, A., and Wendorff, J. H.** (2007). Electrospinning: a fascinating method for the preparation of ultrathin fibers. *Angew. Chem. Int. Ed.*, 46, 5670-5703.
- [15] **Moghe, A.K., and Gupta, B. S.** (2008). Co-axial electrospinning for nanofiber structures: preparation and applications. *Polymer Reviews*, 48, 353-377.
- [16] **Huang, Z.M., Zhang, Y.Z., Kotaki, M. and Ramakrishna, S.** (2003). A review on polymer nanofibers by electrospinning and their applications in nanocomposites. *Composites Science and Technology*, 63, 2223-2253.
- [17] **Tiwari, S. K., and Venkatraman, S. S.** (2012) Importance of viscosity parameters in electrospinning: Of monolithic and core-shell fibers. *Materials Science and Engineering C*, 32, 1037-1042.
- [18] **Beachley, V., and Wen, X.** (2009). Effect of electrospinning parameters on the nanofiber diameter and length. *Materials Science and Engineering C*, 29, 663-668.
- [19] **Url-1** <<http://pubchem.ncbi.nlm.nih.gov/compound/acrylonitrile>>, date retrieved 05.11.2015.
- [20] **Url-2** <<http://ntp.niehs.nih.gov/ntp/roc/content/profiles/acrylonitrile.pdf>>, date retrieved 05.11.2015.
- [21] **Nataraj, S. K., Yang, K. S. and Aminabhavi, T. M.** (2012). Polyacrylonitrile-based nanofibers—a state-of-the-art review. *Progress in Polymer Science*, 37, 487-513.
- [22] **Yördem, O.S., Papila, M., and Menceloğlu, Y.Z.** (2008). Effects of electrospinning parameters on polyacrylonitrile nanofiber diameter: An investigation by response surface methodology. *Materials and Design*, 29, 34-44.
- [23] **Papkov, D., Zou, Y., Andalib, M. N., Goponenko, A., Cheng, S. Z. D. and Dzenis, Y. A.** (2012). Simultaneously strong and tough ultrafine continuous nanofibers. *Acsnano*, Vol. 7:4, 3324-3331.
- [24] **Lin, T., Wang, H., Wang, H. and Wang, X.** (2005). Effects of polymer concentration and cationic surfactant on the morphology of electrospun polyacrylonitrile nanofibres. *J. Mater. Sci. Technol.*, Vol: 21:1, 1-4.
- [25] **McCann, T. J., Marquez, M. and Xia, Y.** (2006). Melt coaxial electrospinning: a versatile method for the encapsulation of solid materials and fabrication of phase change nanofibers. *Nano Letters*, Vol. 6:12, 2868-2872.

- [26] **Chen, C., Wang, L., & Huang, Y.** (2011). Electrospun phase change fibers based on polyethylene glycol/cellulose acetate blends. *Applied Energy*, 88, 3133-3139.
- [27] **Do, C.V., Nguyen T.T.T., and Park J.S.** (2012). Fabrication of polyethylene glycol/polyvinylidene fluoride core/shell nanofibers via melt electrospinning and their characteristics, *Sol. Energ. Mater. Sol. C.*, Vol. 104, 131-139.
- [28] **Url-3** <<http://www.merckmillipore.com>>, date retrieved 17.10.2015.
- [29] **Url-4** <<https://www.sigmaaldrich.com>>, date retrieved 17.10.2015.
- [30] **Url-5** <<https://www.alfa.com>>, date retrieved 17.10.2015.
- [31] **Url-6** < <http://www.goodfellow.com> >, date retrieved 20.10.2015.
- [32] **Guo, J., Xie, P., Zhang, X., Yu, C., Guan, F. and Liu, Y.** (2014). Synthesis and characterization of graft copolymer of polyacrylonitrile-g-polyethylene glycol-maleic acid monoester macromonomer. *J. Appl. Polym. Sci.*, DOI: 10.1002/APP.40152
- [33] **Url-7** < <http://www.yflow.com> >, date retrieved 06.10.2015
- [34] **Li, F., Zhao, Y. and Song, Y.** (2010). Core-shell nanofibers: nano channel and capsule by coaxial electrospinning. *INTECH*, (Vol. 22, pp. 419-435. Retrieved from <http://www.intechopen.com/books/nanofibers/core-shell-nanofibers-nano-channel-and-capsule-by-coaxial-electrospinning>
- [35] **Url-8** <<http://mmrc.caltech.edu/FTIR/FTIRintro.pdf>>, date retrieved 20.09.2015.
- [36] **Url-9**  
<<https://www2.chemistry.msu.edu/faculty/reusch/VirtTxtJml/Spectrpy/nmr/nmr1.htm>>, date retrieved 18.09.2015.
- [37] **Url-10** <<http://teaching.shu.ac.uk/hwb/chemistry/tutorials/molspec/nmr1.htm>,  
<http://process-nmr.com/pdfs/NMR%20Overview.pdf> >, date retrieved 15.09.2015.
- [38] **Url-11** < <http://www.nanoscience.com/products/sem/technology-overview>>, date retrieved 18.09.2015.
- [39] **Hotaling, N. A., Bharti, K., Kriel, H. and Simon Jr, C.G.** (2012). Dataset for the validation and use of DiameterJ an open source nanofiber diameter measurement tool. *Data in Brief*, 5, 13-22.
- [40] **Hotaling, N. A., Bharti, K., Kriel, H. and Simon Jr, C.G.** (2015). DiameterJ: a validated open source nanofiber diameter measurement tool. *Biomaterials*, 61, 327-338.
- [41] **Url-12** <<http://perkinelmer.com>>, date retrieved 05.11.2015.
- [42] **Url-13** <<http://www.joyfay.com/media/import/tester/SNB-1.pdf>>, date retrieved 25.10.2015.
- [43] **Url-14** <<http://www.mrclab.com/Media/Uploads/NDJ-SNB-OPR.pdf>>, date retrieved 25.10.2015.





## CURRICULUM VITAE



**Name Surname** : Ezgi Ceren BOZ NOYAN

**Place and Date of Birth** : 28.01.1990/Hatay

**Address** : Istanbul Technical University, Faculty of Textile Technologies and Design

**E-Mail** : [bozez@itu.edu.tr](mailto:bozez@itu.edu.tr) / [cezgiboz@gmail.com](mailto:cezgiboz@gmail.com)

**B.Sc.** : 2012, İstanbul Technical University, Faculty of Textile Technologies and Design, Textile Engineering, (3.37/4.00)

**M.Sc.** : 2016, İstanbul Technical University, Graduate School of Science Engineering and Technology, Textile Engineering (3.94/4.00)

### List of Publications:

- **E.C. Boz**, E. Önder, “Design of Thermally Adaptive Wool Apparel Fabric”, *2<sup>nd</sup> International Conference on Natural Fibers*, 26-29 Nisan 2015, São Miguel-Azores-Portekiz.
- N. Sarier, R. Arat, **E.C. Boz**, E. Önder, “Biyoesaslı Oleokarbonatların Sentezlenmesi ve Elektroğirme ile Termal Olarak İyileştirilmiş Nanolif Üretiminde Kullanılmaları”, *IV. Uluslararası Polimerik Kompozitler Sempozyumu*, 7-9 Mayıs 2015, İzmir-Türkiye.
- N. Sarier, **E.C. Boz**, R. Arat, E. Önder, “Production of Dynamic Thermal Insulators by Coaxial Electrospinning of PAN and PEG”, *15<sup>th</sup> Autex World Textile Conference 2015*, 10-12 Haziran 2015, Bükreş-Romanya.